INVERSION OF FOCAL MECHANISM DATA FOR THE DIRECTIONS OF STRESS NEAR REDOUBT VOLCANO, ALASKA

By

John Jairo Sánchez Aguilar

RECOMMENDED:

Dr. Max Wyss

Dr. Seth C. Moran

Dr. James E. Gardner

Dr. Douglas H. Christensen

Dr. Stephen R. McNutt, Chairman Advisory Committee

Dr. Paul Layer, Head, Dept. of Geology and Geophysics

APPROVED:

Dr. David M. Woodall, Dean, College of Science, Engineering, and Mathematics

Dr. Joseph R. Kan, Dean of the Graduate School

12-1-00

Date

INVERSION OF FOCAL MECHANISM DATA FOR THE DIRECTIONS OF STRESS NEAR REDOUBT VOLCANO, ALASKA

A

THESIS

Presented to the Faculty

of the University of Alaska Fairbanks

in Partial Fulfillment of the Requirements

for the Degree of

MASTER OF SCIENCE

By

John Jairo Sánchez Aguilar, B.S.

Fairbanks, Alaska

December 2000

ABSTRACT

Fault plane solutions (FPS) of 308 earthquakes, with largest magnitude of 2.1, occupying a 16 km^3 volume below 6 km depth, were inverted for principal stress directions near Redoubt volcano, during 1989-1991. On average, FPS were computed with 9 P-wave readings, inversions performed with 50 FPS, yielding misfits of 6.5° and, the size of the 95% confidence regions of stress directions is 30°. During the 1989-1990 eruptions, stresses were typically: sub-horizontal σ_1 and σ_2 striking SE-NW and SW-NE, respectively, and near-vertical $\sigma 3$; whereas in July 1991 we found: near-vertical σ_1, and sub-horizontal σ_2 and σ_3 striking SE-NW and SW-NE, respectively. We found differences in plunge of σ_1, up to 68°, between 1990 and 1991, and subvolumes with different stress at the 99% confidence level, evaluated with the *z* test. We speculate that expansion and contraction of a magma body increased and subsequently reduced the stresses at Redoubt.

Table of contents

List of Figures

List of Tables

List of Appendices

Acknowledgments

I want to thank my adviser Dr. Stephen R. McNutt who helped me since my arrival to Alaska in many aspects of my learning process. With patience and constant encouragement he showed me how to become excited in research of Alaskan volcanoes an helped me forget about the not-so-nice cold winter in Fairbanks. He also encouraged me to share experiences with other researchers during a meeting in Mexico. Many thanks to professor Max Wyss who acquainted me with the methods of stress inversion and cumulative misfit, and followed closely many parts of the work. His help and dedication improved greatly my research of focal mechanisms and stress at Redoubt. I also thank professors Douglas Christensen, James Gardner and Dr. Seth Moran who served in my advisory committee and helped me throughout my academic process.

My stay in the U.S. during the last two years was supported by a COLCIENCIAS/FULBRIGHT scholarship and the funds were administered by IIE (Institute of International Education). Many thanks to COLCIENCIAS staff and Dr. Catherine Leiva (IIE) who advised me since my arrival to UAF. Also part of my funding was provided by a Research Assistanship from the University of Alaska, Fairbanks and the Geophysical Institute. I am also Indebted to all the fellows at the Alaska Volcano Observatory and the department of Geology and Geophysics at UAF who helped me many times when I had questions and needed assistance. Mitch Robinson provided lots of

help with software and data file conversion, Stefan Wiemer provided assistance using ZMAP, Natalia Ratchkovski introduced me to the FPFIT program for focal mechanisms and the GMT software, many thanks to them. John Lahr, John Power, David Oppenheimer and Kent Fogleman advised me in different aspects of the work. Mary Edmunds from IRIS-DMC kindly provided the data collected during the 1991 deployment at Redoubt. No doubt that my wife deserves all credit for being so lovely and patient. I really admire her because she is able to be calm and understanding when I am focused at work.

1. Introduction

Seismic signals recorded at volcanoes have been used extensively to model processes that occur before, during, and after eruptions, in terms of the types of earthquakes, temporal and spatial distributions of seismicity, seismicity rates, and energy release. Volcano-tectonic earthquakes (also referred to as high-frequency or A-type earthquakes) are a particular example of such signals. They are characterized by sharp onsets, dominant frequencies between 5-15 Hz, clear P and S phases (Minakami, 1960; McNutt, 1996; Power et al., 1994), and typically occur at 0-10 km depth beneath volcanoes. Source mechanisms for these earthquakes, however, remain understudied, in part due to the complexity of processes that take place in earthquake generation and also because of the intrinsic limitations of volcano monitoring.

Data gathered at the Alaska Volcano Observatory (AVO) during years of monitoring have been used to investigate many interesting aspects of the behavior of volcanoes, and in several cases, valuable data have been recorded during eruptive episodes. One of those episodes occurred at Redoubt volcano, located in south-central Alaska, which erupted between December 1989 and June 1990 in a series of events that included tephra eruptions, pyroclastic flows, lahars, and debris flows, and episodes of dome growth and destruction (Power et al., 1994; Miller, 1994). The eruption sequence was monitored by a network of five to nine seismographs stations located within 22 kilometers of the vent,

and various features of it included; changes in type of seismicity with time, changes in intensity of seismic swarms, and the identification of different depths of occurrence of volcano-tectonic events related to different stages of activity. The analysis of the seismic sequence allowed an interpretation of both the processes that led to the eruption and the geometry of the magmatic system (Power et. al, 1994, Chouet et al., 1994). No work, however, has been done on the focal mechanisms associated with the volcano-tectonic events or the stress regime that could be involved in their generation.

In this thesis, earthquake first motion data recorded at Redoubt volcano between December 1989 and December 1990 by the AVO permanent network, and during July 1991 by a temporary array of 21 digital stations, have been used to compute focal mechanisms. These were inverted for the directions of principal stress axes following the method of Gephart and Forsyth (1984). Using a misfit analysis (Lu and Wyss, 1995), we attempt to identify different subsets of earthquakes near the volcano that have been generated by different stress regimes.

2. Background

Redoubt volcano is a steep-sided stratovolcano, about 10 km in diameter at its base with a volume of 30-35 km^3, located near the eastern end of the Alaska-Aleutian volcanic arc (figure 1). The volcano is composed of intercalated pyroclastic deposits and lava flows resting on Mesozoic rocks of the Alaska-Aleutian range batholith (Till et al., 1994). The most recently active vent is located on the north side of the crater.

Eruptions have occurred at Redoubt volcano many times this century, with the oldest historic eruption in 1902 (Martin and Katz, 1912). Vapor emissions were reported in May 1933, and January-February, 1965. During late January and early February, 1966, an explosive eruption produced ash plumes as high as 6100 m (Sturm et al., 1986). The eruptive sequence that began in December 1989, was preceded by a 23- hour swarm of long-period seismic (LP) events, indicative of pressurization of the magma system (Chouet et al., 1994). Volcano-tectonic (VT) activity, reflecting stress changes in the volcanic edifice in response to magma movement, was initially confined to shallow depths (in the range 0-3 km) beneath the summit, but shifted to greater depths (6-10 km) during the second day of the eruption sequence (Power et al., 1994). Spatial changes in VT and LP activity reflected dynamic changes within the volcano associated with migration and pressurization of magmatic fluids (Chouet et al., 1994; Stephens et al., 1994). Seismicity declined after June 1990, and remains at low levels as of this writing.

The method of inversion for stress directions from fault plane solutions (FPS) has not been tested at volcanoes, and no previous attempt has been made to study the focal mechanisms or the stress field at Redoubt. With a study of VT activity and the search for the directions of principal stress axes, therefore, we expect to contribute to a better understanding of the stress field at volcanoes during and after eruptions.

3. Volcanology of the Eruptions

3.1. Summary of Volcanological Aspects of the Eruptions.

More than 20 eruptive events during the 1989-1990 eruptions emplaced a sequence of lithic pyroclastic-flow, -surge, -fall, ice-diamict, and lahar deposits, mainly on the north side of the volcano. The deposits record the change in eruption dynamics from initial, gas-rich, vent-clearing explosions to episodic, gas-poor, lava-dome extrusions and failures (Gardner et al., 1994). Tephra plumes rose to altitudes of 7 to more than 10 km, and were carried mainly northward and eastward by prevailing winds, seriously impacting air travel, commerce, and other activities (Scott and McGimsey, 1994). The total volume of tephra-fall deposits (dense-rock equivalent) was estimated to be 3-5 x 10^7 m^3 of andesite and dacite. Two contrasting tephra types were generated; pumiceous tephra-fall deposits from December 14 and 15, and fine grained, lithic-crystal tephra deposits from December 16 and all later events. The different character of tephra-fall deposits reflects differences in their modes of origin. Pumiceous deposits were produced by magmatically driven explosions, whereas the fine-grained lithic-crystal deposits were generated by hydrovolcanic vent explosions and ash clouds of lithic pyroclastic flows.

Much of the 1989-1990 eruption consisted of a dome-growth and -destruction phase

in which 14 short-lived, viscous, silicic andesitic domes were emplaced and subsequently destroyed. The duration of an individual dome ranged from 3 to 21 days, and volumes are estimated at 1 $x10^6$ to 30 $x10^6$ m^3 (Miller, 1994). Magma supply rates to the vent area averaged about 5 $x10^5$ m^3/day for most of the dome-building phase, ranging from a high of 2.2 $x10^6$ m^3/day initially to a low of 1.8 $x10^5$ m^3/day at the final stages of the eruption. The total volume of all domes was estimated to be about 90 $x10^6$ m^3, and may represent as much as 70% of the volume for the entire eruption (Miller, 1994). The repeated dome failures produced lithic pyroclastic flows that mixed snow and ice generating lahars that were channelled into the Drift River valley. Some of the dome failures occurred without precursory seismicity, and appeared to have resulted solely from gravitational instability (Scott and McGimsey, 1994). Most of the dome-collapse events resulted in single, monolithologic, massive to reversely graded, medium-to-coarse-grained, pyroclastic flow deposits containing abundant dome clasts. The deposits vary in thickness, grain size, and texture, depending on the distance from the vent and local topography. Deposits are finer and better sorted downstream, thinner and finer on hummocks, and thicker and coarser where ponded in channels cut through the glacial ice. The deposits had an estimated volume of 0.04 km^3 (Scott and McGimsey, 1994).

4. Instrumentation and Data Used in this Study

Five to nine high-gain, short-period seismograph stations, located within 22 km of the volcano's summit, provided the data used to monitor the 1989-1990 eruptive sequence (figure 2a). Until AVO was established, only two stations were operated in the Redoubt area; RDT (three-component), installed in 1971, and RED, installed in 1974. In October 1989, DFR, NCT, and RDN began operation as part of the monitoring program. These five stations operated during the initial phases of the eruption. DRE was installed on February 1, 1990, both to improve monitoring of the seismicity and to detect lahars and mud flows in the Drift River valley. To enhance the network's detection of small events within the volcanic cone, stations RSO, REF, and RWS were installed in March 1990, and RDW replaced RWS in September 1990 (Power et al., 1994). We selected VT earthquakes recorded between December 1989, and December 1990, located with a minimum of 6 P- wave arrivals to compute FPS. A typical earthquake waveform from this data set is shown in figure 2b.

During July 1991 an array of 21 digital seismometers was deployed on Redoubt volcano (Dawson et al., 1996). The goal of this deployment was to record local and regional seismic events and four explosions in order to improve the existing 1-D velocity model. PASSCAL (Program for Array Seismic Studies of the Continental Lithosphere) REF-TEK model 72A digital recorders and geophones were used. A detailed description

of the REF-TEK model 72A portable seismic data acquisition system can be found in Refraction Technology, Inc. (1990). The recorder can collect up to 16 channels of data with sampling rates of 1 to 1,000 per second with 16-bit resolution. Mark Products™ three-component L-22-3D seismometers, with natural frequency of 2 Hz and sensitivity of 0.5 V/cm/s, were used. Digital data and locations of earthquakes were provided by IRIS (Incorporated Research Institutions in Seismology). The recorders were deployed in three semi-linear arrays across the volcano and in a diffuse pattern to fill empty spaces between the AVO permanent network stations (figure 3a). Seismicity recorded during the three weeks of operation included 240 VT events, several hundred regional events, hundreds of glacier quakes, several teleseisms, and thousands of small microearthquakes. The XPICK program (Robinson, 1991), coupled with HYPOELLIPSE (Lahr, 1999), was used to locate the events. As with the AVO data set, we selected events usually located with more than 6 P-wave readings to compute FPS. A typical VT earthquake recording acquired with this network is shown in figure 3b. The improved 1-D velocity model resulting from the experiment (Dawson et al., 1996) did not differ greatly from the velocity model that was in use during 1989-1990, and although the accuracy in locations apears to be higher (see appendix A) there was no effect on the resultant FPS.

4.1. Description of Seismicity at Redoubt Volcano During December 1989 - December 1990

Earthquakes at Redoubt volcano were concentrated mostly in a region elongated in a NW direction and located north and east of the volcano. In addition, clusters of seismicity are located northeast, east, and southeast of the volcano (figure 4a). Magnitudes (*ML*) of events are in the range –0.9 [ML [2.1, with depths (*Z*) between 0 and 11 km, with a prominent cluster located between 6 and 9 km (figures 4b, c). The depths are referenced with respect to the summit crater floor, which is 2.3 km above sea level. The average horizontal and vertical formal errors in locations (as furnished by HYPOELLIPSE) are 0.9 and 1.8 km, respectively. The largest event in this period was a magnitude *ML*=2.1 that occurred on January 2, 1990, at a depth of 7.8 km. Most of the events located between 0 and 3 km depth occurred in a short time interval following the large tephra eruptions on December 15, 1989.

Events in the range 6 - 10 km occurred late on December 15 and continued throughout and after the eruption. Volcano-tectonic events are assumed to result from brittle failure of rock caused by stresses generated by magma movement. The distribution of hypocenters suggess a magmatic system consisting of a deep source region connected to the surface by a thin conduit (Power et al., 1994). The fact that events in the 6-10 km depth range began occurring only after the vent-clearing tephra eruptions of December 15 suggests that these earthquakes are associated with stress readjustments caused by the

movement of magma and volatiles at those depths. A northward migration of deeper VT events observed between March and October 1990 suggests that the deep magma source region may be a tabular volume elongated to the north (Lahr et al., 1994). It is speculated that this migration resulted from readjustment of stress, as successively greater portions of the source region depressurized (Power et al, 1994). Most shallow VT events occurred in association with the tephra eruptions of December 1989. These events are thought to represent readjustments of stresses in the wall rock in response to depressurization of the upper portions of the magmatic system, caused by removal of magma and volatiles from these depths (Power et al., 1994).

4.2. Description of Seismicity Recorded During the Deployment in July 1991.

Seismicity recorded with the array deployed during July 1991 showed an epicentral distribution similar to that of the 1989-1990 period, with earthquakes located mostly north of Redoubt within a depth range of 0–10 km. The earthquakes do not show any particular alignment (figure 5a). E-W and N-S cross-sections show that most of the earthquakes occur in the depth range 5–9 km (figures 5b, c). Magnitudes vary between 0 and 1.1. The average formal horizontal and vertical location errors are 0.38 and 0.66 km, respectively.

5. Fault Plane Solutions at Redoubt

Fault plane solutions were computed with FPFIT, a program by Reasenberg and Oppenheimer (1985) which performs a two-stage grid-search procedure to find the double-couple model that minimizes a normalized weighted sum of first-motion polarity discrepancies. For each FPS obtained, the program formally computes the uncertainty in the model parameters (strike, dip, rake) and a parameter called the Station Distribution Ratio (STDR); this quantity is sensitive to the distribution of the data on the focal sphere, relative to the radiation pattern. When this ratio has a low value (STDR < 0.5), then a relatively large number of data points (stations) lie near the nodal planes of the solution, meaning that the P-wave arrivals to these stations may be emergent and therefore the polarities are difficult to identify. For a description of the STDR parameter and other features of FPFIT code, the reader is referred to Reasenberg and Oppenheimer (1985). FPFIT also gives a stereo projection of all orientations of P and T axes compatible with the available data. We also computed the quantity NDisc/NPol (NDisc is the number of violations or discrepant observations and NPol is the number of first readings used in the solution) and used its value to set another constraint on the acceptability of a FPS for analysis.

Using the features described from the FPFIT code and the quantity NDisc/NPol, we eliminated FPS if they met any one of the following criteria:

-The quantity STDR was equal to or greater than 0.4.

- The averaged uncertainties in strike, dip, and rake (ΔStrike, ΔDip, ΔRake) were greater than or equal to 45°.

- The ratio NDisc/NPol was greater than 0.20.

- The uncertainty in P and T axis orientations was so large that the regions overlapped.

These criteria significantly reduced the number of FPS, leaving a sample of 96 FPS from the located seismicity in July 1991, and 212 events recorded with the AVO permanent network between 1989 and 1990. Appendix A summarizes the values of parameters used in the selection of FPS from each data set.

5.1. Fault Plane Solutions from December 1989 to December 1990.

The computed FPS for earthquakes near Redoubt during the period December 1989 - December 1990 show a variety of mechanisms. For convenience, we show FPS computed for each of the four stages of activity at Redoubt described by Power et al. (1994); 1) vent clearing and first dome-building phase, 2) second dome-building phase, 3) repetitious dome-building phase, and 4) post-eruption phase.

For events from the vent-clearing and first dome-building phase, we observe normal faulting with near-vertical P-axes, and reverse faulting with near-horizontal P-axes

oriented E-W to SE- NW; a rose diagram shows that strikes of nodal planes are mostly oriented N-NE and W-NW (figure 6a). Earthquakes during the second dome-building phase show some normal faulting with near vertical P-axes oriented NW; reverse faulting with P-axes oriented NW, strike-slip faulting with P- axes oriented NW, and several vertical dip-slip events with P-axes oriented also NW; the strikes of nodal planes are mostly oriented NNE and SSW (figure 6b). Events during the repetitious dome-building phase show some normal faulting with near vertical P-axes, strike slip with P-axes oriented NW, and reverse faulting with P-axes oriented N-S, and NW; the rose diagram shows that many nodal planes strike WSW and NW-NE (figure 6c). During the post-eruption phase we observe some normal faulting with near-vertical P-axes, strike-slip faulting with P-axes oriented E-W to NW, and reverse faulting with P-axes oriented NW; the rose diagram shows nodal planes striking mostly NNE and S (figure 6d). Throughout most of the 1989-1990 period we observe that FPS are dominantly reverse and strike-slip, with P-axes oriented mostly NW.

5.2. Fault Plane Solutions from July 1991

Fault-plane solutions for shallow earthquakes (defined in this thesis as those events with depths in the range 0-6 km), located directly north of Redoubt, show normal faulting with near-vertical to vertical P-axes, strike slip faulting with P-axes oriented NW and E-W, and reverse faulting with P-axes striking NW; the strikes of nodal planes in this depth

range show a high variability, with no preferred orientation (figure 7a). Earthquakes in the range 6 to 11 km show mainly normal faulting, with near-vertical P-axes. Several events show strike slip and vertical dip-slip faulting with P-axes oriented NW, NE, and N, a few events showed strike-slip with some reverse component, and P-axes oriented NE; the orientation of nodal planes is mostly SE-NW (figure 7b). A striking feature of seismicity near Redoubt during July 1991 is that most events show normal faulting with near-vertical P-axes. This contrasts with FPS during 1990, in which we observed mostly reverse faulting (compare figure 6c-d with 7b).

6. Stress Tensor Inversion

To find the directions of stress we follow the method of Gephart and Forsyth (1984), which uses FPS of earthquakes as input data. The method is based on the following basic assumptions: (1) stress is uniform in the rock volume sampled by the seismicity; (2) earthquakes are shear dislocations on pre-existing faults; and (3) slip occurs in the direction of the resolved shear stress on the fault plane. The algorithm finds a best fitting principal stress tensor to a group of earthquakes by performing a grid search over a range of possible models. The parameters of the stress tensor obtained from the inversion scheme are the directions of the maximum (σ_1), intermediate (σ_2), and minimum (σ_3) principal stress axes, and a measure of their relative magnitudes (R), where $R = (\sigma_1 - \sigma_2)/(\sigma_1 - \sigma_3)$. Also computed is the parameter ϕ, which is the rake of σ_2 in the plane normal to σ_1; its value is such that it is 0 when σ_2 is horizontal, and positive when σ_2 plunges to the west.

A misfit variable is introduced to define discrepancies between the stress tensor and the observed FPS. The individual misfit, f, is defined as the smallest rotation angle about an axis of any orientation that would bring the direction and sense of slip, associated with either of the two nodal planes, into agreement with the direction and sense of slip predicted by the stress model. Each FPS receives two misfits, one for each nodal plane. If

an *a priori* choice of fault plane is not made, then the nodal plane with the smallest misfit is assumed to be the fault plane. The algorithm also computes the statistical confidence limits for possible stress orientations, based on a procedure described by Parker and McNutt (1980). The confidence limits that are consistent with a set of FPS can provide additional information on stress heterogeneity because, in general, they tend to enlarge when the heterogeneity in stress increases. This can also depend on the number of FPS, at least for small data sets (15-20 FPS). Recently, a study by Hardebeck and Hauksson (2000) revealed that the method of Gephart and Forsyth (1984) usually provides more accurate estimates of stress orientation, specially for high-quality data sets, but its confidence regions are, in most cases, too large. A method by Michael (1987) is more accurate for noisy data sets and gives a more appropriate estimate of uncertainty. Since in most cases we obtained inversion results with confidence regions that do no overlap, we feel confident that the solutions are well constrained and their confidence regions could be even smaller.

Caution must be exercised when interpreting the results of the inversion method, because if the data used come from several regions with significantly different stress orientations we could obtain a composite stress tensor and not identify it as such (Lu and Wyss, 1996). We must then make an effort in identifying portions of the data that can be called homogeneous. There exists the uncertainty as to how much of the average misfit, F, is contributed to by errors in the FPS and how much by heterogeneity in the stress field. The portion of the average misfit that could result from FPS errors of approximately

15° has been estimated to range as high as 6° based on tests with synthetic data (Wyss et al., 1992; Gillard and Wyss, 1992; Lu et al., 1997). Values of $F \leq 6°$ have been explained by reasonable errors in FPS, and so we will accept results with $F \leq 6°$ as satisfying the homogeneity criteria. On the other hand, inversions with F in the range $6° < F < 9°$ are considered acceptable, but containing some heterogeneous data (Giampiccolo et al., 1999). A solution with $F > 9°$ will be regarded as representative of a non-homogeneous stress field. Based on these considerations, Lu and Wyss (1996) proposed that if subsets of earthquakes, as a function of space or time, can be obtained by dividing the entire data set with the result of a substantial reduction of F, we can conclude that part of the initial misfit was caused by heterogeneities. Often times an inversion of a group of FPS results in average misfits larger than 9°, yet the confidence regions for stress orientations are small and do not overlap. In these cases, based on tectonic considerations, such as clustering or alignment of epicenters, tectonic models, and variations of activity with time, we subdivide our data set and perform independent inversions for each subset in order to find average misfits that are more likely representative of a homogenous sample.

6.1 The Cumulative Misfit Method

To investigate stress homogeneity along plate boundaries and faults, Wyss and Lu (1995) and Lu and Wyss (1996) proposed the cumulative misfit method. The technique is based on the cumulative misfit of individual FPS calculated using test-stress tensors. The

method has been successfully used in identifying segmentation in the Aleutian plate boundary (Lu and Wyss, 1996) and the San Andreas fault (Wyss and Lu, 1995), and time variations of stress in Friuli, Italy, (Slejko et al., 1999). The method, however, has not been tested in volcanic areas, where variations in stress over short distances and time intervals may be expected.

The method works as follows: we assume that stress in a region is heterogeneous as a whole, but can be considered homogeneous in subvolumes. The purpose is to find where stress changes may be located. We use as a test-stress tensor the model that fits either a subgroup of FPS or the assumed tectonic stress, as indicated by a small average misfit and small confidence regions, and then compare the individual misfit of each FPS with respect to that test-stress tensor. We order the earthquakes sequentially by increasing time, increasing depth, or increasing latitude, and plot the cumulative misfit as a function of earthquake number to identify boundaries between regions of different stress, or the points where a change in slope occurs. The statistical significance of the difference in stress across a boundary between two segments is quantified by the standard z test, if the number of samples (n) is greater than 30, or by the t test if $n < 30$. We apply the cumulative misfit method, and test the hypothesis that variations in the stress field exist underneath Redoubt volcano, not only in time, but also in space.

6.2 Stress Inversions at Redoubt Volcano 1989-1990

FPS of earthquakes at Redoubt volcano from December 1989, to December 1990, were used to invert for stress tensors and to investigate possible changes in stress field with time. Following the method of Gephart and Forsyth (1984), we inverted the entire data set of 212 FPS to test the hypothesis that all rupture geometries could be explained by a single uniform stress tensor. The result of this test is shown in figure 8. It is a stereographic projection of the range of possible orientations of the principal stress axes. Also shown are the computed values of R, ϕ, and F, along with a histogram showing the distribution of R values.We see that although the solution is well constrained, because 95% confidence regions for the principal stress directions are small and do not overlap, the average misfit is large (F=9.4°), which means that it does not fulfill the initial assumption of stress homogeneity. This is expected, given that the data set includes events from the 1989-1990 eruption and from a period of low level activity, and also spans a relatively large area around the volcano. Since our initial solution is well constrained, we can expect that subdivision of our data set into smaller groups will give solutions with smaller misfits. We next look for a solid criterion for subdividing the data into coherent groups. To achieve this goal we use the cumulative misfit method, which has proven to be useful in the identification of stress-homogeneous subvolumes.

6.2.1. Stress Near Redoubt as a Function of Time

To investigate how the state of stress behaves in time near Redoubt volcano we use ZMAP (Wiemer and Zuñiga, 1999) to map the individual misfits of all 212 FPS during 1989-1990 as compared to the following stress model: σ_1=8/297, σ_2=48/199, σ_3=41/34 (plunge/azimuth), R=0.7, and ϕ=-49. This model is assumed to be similar to the tectonic stress based on previous work by other researchers (Nakamura et al., 1977; Jolly et al., 1994). A map view and NW- oriented cross-section of epicenters are shown in figure 9. There is a significant variation in misfits throughout the area sampled, with misfit values in the range 0.1° to 45° (small and black symbols mean small misfits, whereas large and light grey symbols mean large misfits). In general, we observe small to large misfits for the main cluster of seismicity (north of Redoubt) and moderate to large misfits for earthquakes scattered around the main cluster.

Next, we plot the cumulative misfits of our FPS, compared with the above test tensor, against earthquake number ordered by time (figure 10). There are several changes in slope, defining phases that are identified at the 99% confidence level. The first important change in slope occurs at earthquake number 16 (January 31, 1990, 03:28), the second change occurs at earthquake number 68 (March 8, 1990, 13:00), and the third change is identified at earthquake number 179 (June 6, 1990, 9:07). The relevant information about the phases is summarized in table 1.

Table 1. Description of Phases in Figure 10.

Phase	FPS	Time range	Average of individual misfits (degrees)	Confidence level at which phase is different from neighbor
1	1-15	12/15/89-01/31/90	19	99%
2	16-67	01/31/90-03/08/90	12	99%
3	68-178	03/08/90-06/01/90	19	99%
4	179-212	06/08/90-12/24/90	9	

The analysis of segments in curves of cumulative misfit will be considered successful if the inversions for the stress directions in the individual segments give average misfits F_i that are less than 6° and also if F_i is significantly lower than F for the total data set (Wyss and Lu, 1995). Within each segment we perform separate inversions; first we include all events in the segment and, if possible, we select a subset and perform another inversion.

From phase 1, we obtain the solution displayed in figure 11a. The solution is not well constrained, because the confidence regions for σ_2 and σ_3 overlap. The average misfit of 6.9° indicates that the FPS used contain some heterogeneity. We do not subdivide this group of only 15 FPS. Figure 12a shows the map of individual misfits for events in phase 1.

The inversion of all events in phase 2 gives a well-constrained solution, with an average misfit of 5.7 °, a horizontal σ_1 striking nearly E-W, a near-vertical σ_2, and a near-horizontal σ_3 striking nearly N-S (figure 11b). Although F is less than 6° and may be accepted as representing stress homogeneity, we select a subset of events that are spatially close for a second inversion (figure12b). The 34 FPS in this phase, include only earthquakes clustered NW of the summit in the depth range 6 to 8 km. Their inversion gives a well constrained solution, with average misfit of 3.6°, a sub-horizontal σ_1 striking NW-SE, a near-horizontal σ_2 striking NE-SW, and a near-vertical σ_3 (figure 11c). Note the changes in σ_2 and σ_3 from figure 11b.

The inversion of all events in phase 3 gives a solution, with an average misfit of 7.9°, a near-horizontal σ_1 striking SE-NW, a near-horizontal σ_2 striking NE, and a steeply plunging σ_3 (figure 11d). We selected a subset of 86 earthquakes that are closely located (figure 12c), and the solution is similar to that for the whole segment, with a misfit of 6.5°, suggesting that some heterogeneity persists in the subset set (figure 11e).

By inverting all earthquakes in phase 4 we obtained a solution with an average misfit of 6.8°, a near-horizontal σ_1 striking nearly E-W, a near-vertical σ_2, and a horizontal σ_3 striking nearly N-S (figure 11f). This value decreased to 4° after we reduced the number of FPS to 19 by selecting earthquakes located close to each other (figure 12d), and the directions of stress axes appear slightly changed (figure 11g). Figure 12a-d shows the maps of individual misfits for events within each segment of figure 10. Table 2 summarizes the relevant aspects of the inversion results for each phase.

Table 2. Inversion Results for Individual Phases in Figure 10.

Phase	Number of FPS submitted for inversion	F (degrees)	Principal stress directions (best fitting tensor) plunge/azimuth σ_1, σ_2, σ_3	R	ϕ (degrees)
1	15	6.9	18/126, 71/135, 6/128	0.2	-84
2	52	5.9	4/277, 70/19, 20/186	0.5	70
2	34	3.6	19/317, 25/55, 61/189	0.5	22
3	111	7.9	10/107, 39/9, 42/209	0.3	-39
3	86	6.5	10/107, 39/9, 49/209	0.2	-39
4	34	6.8	19/96, 73/261, 4/5	0.4	85
4	19	4	5/117, 28/210, 61/18	0.6	28

In figure 10 we have superimposed red lines to indicate the limits between different stages of activity during the 1989–1990 eruptive sequence, as described by Power et al. (1994). We observe that most phases in this curve of cumulative misfit vs. time are closely associated with changes in activity at Redoubt, with the most striking match

occurring between the beginning of segment 4 and the change between stages D and E (the repetitious dome-building and post-eruption stages).

6.3. Stress Inversions July 1991

We use a set of 96 FPS from events recorded during July 1991, a period of low activity level (figure 5), to investigate the stress field near Redoubt as a function of space. We want to test the hypothesis that all FPS during July 1991 can be explained by a single uniform stress tensor. Following the same approach described for the time analysis, we attempt an inversion of the full data set. The result of this first trial is shown in figure 13. As expected, the solution is well constrained, but the misfit is large, indicating that the data are heterogeneous. Since our initial solution is well constrained, we expect that dividing our data set into smaller groups can give solutions with smaller misfits. Again, we will make use of the cumulative misfit analysis to select subsets of data that can give meaningful inversion results.

6.3.1. Stress Near Redoubt as a Function of Space

To investigate possible variations of stress as a function of space near the volcano, we map the individual misfits of all 96 FPS in July 1991 as compared to the same tectonic stress model used for the time analysis: σ_1=8/297, σ_2=48/199, σ_3=41/34 (plunge/azimuth), R=0.7, and ϕ=-49. A map view and a NW-oriented cross-section of individual misfits are shown in figure 14. We see that there is a great deal of variation in misfits throughout the area sampled, with misfit values in the range 0.3° - 44°. Large misfits appear to be concentrated in a region between 60.50° N - 60.53° N and 152.78° W - 152.73° W, and surrounded by large misfits. A trend in individual misfits with depth is not manifest in the cross-sections

We next plot cumulative misfits against earthquake number, ordered by increasing depth (figure 15). There is an evident change in slope that takes place at earthquake number 22. The shallow earthquakes (0 - 6.4) km have the lowest slope, indicating close agreement with the test tensor. After that point, the curve switches to a higher slope, which indicates that earthquakes in this segment diverge from our test tensor. Applying the z test, we find that the slopes of the segments are significantly different at the 99% confidence level. The fact that the two segments (table 3) are significantly different in a statistical sense confirms the differences in misfit with depth.

Table 3. Description of Segments in Figure 15.

Segment	FPS	Depth range (km)	Average of individual misfits (degrees)	Confidence level at which phase is different from neighbor
1	1-22	0-6.4	14	99%
2	23-96	6.4-11	24	

We proceed to run separate inversions for FPS within individual segments, first using all events in the segment and then using events from restricted volumes. The results of inversions of FPS within individual segments are described in table 4. By inverting all events in segment 1 we found a well constrained solution with an average $F = 8.9°$, a near-horizontal σ_1 striking SE-NW, a near-vertical σ_2, and a near-horizontal σ_3 striking SW-NE (figure 16a). In search of a stable solution (one that has smaller average misfit) we attempted to find a smaller subvolume with enough events to attempt an inversion for stress directions. Most events within segment 1 are located in a cluster between 152.7°W - 152.74°W and 60.49° N - 60.51° N (figure 17a). Rejecting the events outside this region, we obtain a subgroup of 17 events. Their inversion yielded a well constrained stable solution with $F = 6.8°$. Although F was reduced by 2 degrees, its absolute value tells us that the solution still reflects some degree of heterogeneity. This may result from the cluster containing events from different depths (0-3, 3-6 km), and the FPS in each group may be

explained by stress tensors that differ. We do not attempt to further subdivide this subset because the minimum number of FPS required for a stable inversion is 15. We regard this solution as acceptable, but containing some heterogeneity.

The inversion of all FPS within segment 2 gives an average misfit of 6.8°, a near-vertical σ_1, a near-horizontal σ_2 striking SE-NW, and a near-horizontal σ_3 striking NW-SE (figure 16c). With the help of the misfit map and cross-section (figure 17b) we select 39 earthquakes clustered between 6.5 and 8.5 km and between 3.8 and 6 km from point A. Their inversion gives a well constrained solution with a misfit of 4.5°, a near-vertical σ_1, a near-horizontal σ_2 striking SE-NW, and a near-horizontal σ_3 striking SW-NE (figure 16d). We regard this solution as representing a homogeneous stress tensor. We note that the stress orientations found for segment 2 have reversed σ_1 and σ_2 with respect to segment 1 (figure 16b). This reversal could be an indication of a rotation of stress directions with depth near Redoubt volcano.

Table 4. Inversion Results for Individual Segments in Figure 15.

Segment	Number of FPS submitted for inversion	F (degrees)	Principal stress directions (best fitting tensor) plunge/azimuth σ_1, σ_2, σ_3	R	ϕ (degrees)
1	22	8.9	27/136, 62/339, 10/231	0.2	-79
1	17	6.9	27/136, 62/339, 10/231	0.2	-79
2	74	6.8	74/29, 16/205, 1/296	0.5	86
2	39	4.5	73/30, 8/150, 14/242	0.7	30

We next plotted the cumulative misfit against earthquake number by latitude (figure 18). The results of inversions of FPS within individual segments of figure 18 are summarized in table 6. A change in slope of the curve is evident at earthquake number 25 (latitude 60.5° N), where the slope becomes higher and continues with the same trend, with some small steps, until earthquake number 96. The z test analysis of the observed change in slope is summarized in table 5.

Table 5. Description of Segments in Figure 18.

Segment	Earthquakes	Average misfit (degrees)	Latitude interval	Confidence level at which segment is different from neighbor
1	1-24	15	60.436°N-60.501°N	99%
2	25-96	24	60.501°N-60.553°N	

Having identified at least two segments with different slopes in figure 18, we inverted FPS of events within each segment, first using all events in the segment, and by selecting them according to their individual misfits and locations. For segment 1, we obtained for all FPS by inverting all FPS, a solution with large confidence regions (but no overlap), an average misfit of 9.1°, a near-vertical σ_1, a near-horizontal σ_2 striking SE-NW, and a near-horizontal σ_3 striking NE-SW. The average misfit for this set of events is indicative of heterogeneity in the sample (figure 19a). By inverting a subset of 16 events (figure 19b) we found an improved solution that also has large confidence regions with a near-horizontal σ_1 striking SE-NW, a steeply plunging σ_2 striking NW-SE, and a near-horizontal σ_3 striking NE-SW. Because the average misfit obtained for this subset is 6.3°, we accept it as containing a small amount of heterogeneity.

The inversion of all FPS for segment 2 (72 total events) shows a well constrained set of confidence regions, an average misfit of 7.5°, a near-vertical σ_1, a horizontal σ_2

striking SE- NW, and a near-horizontal σ_3 striking SE-NW. The average misfit is again indicative of heterogeneity in the sample (figure 19c). Inversion of 46 events clustered NW of Redoubt (between 152.78° W and 152.4° W, and 60.501° N and 60.53° N) leads to a reduced average misfit of 5.6° with a near-vertical σ_1, a near-horizontal σ_2 striking SW-NE, and a horizontal σ_3 striking SE-NW (figure 19d). We note that between segment 1 and 2 the orientations of, σ_2 and σ_3 principal stress axes are switched, whereas the orientation of σ_1, remains the same. This fact, along with the distribution of R values, tells us that σ_2 and σ_3 must have similar magnitudes.

Figure 20a-b shows the maps of individual misfits for events within the two segments identified in the cumulative misfit vs. latitude curve. The results of analyzing the change of cumulative misfit as a function of latitude give us basis to suggest that differences in stress exist between earthquakes located south and north of 60.501° N in the Redoubt volcano area, with southerly events characterized by a heterogeneous stress field, and northerly events by a mostly homogeneous stress field.

Table 6. Inversion results for individual segments in figure 18.

Segment	Number of FPS submitted for inversion	F (degrees)	Principal stress directions (best fitting tensor) plunge/azimuth σ_1, σ_2, σ_3	R	ϕ (degrees)
1	24	9.1	71/251, 15/109, 11/16	0.6	-53
1	16	6.3	38/147, 47/294, 17/43	0.6	68
2	72	7.5	73/30, 7/146, 15/238	0.7	26
2	34	5.6	75/177, 12/31, 8/299	0.3	-56

6.4. Summary of Results

The results of inversions of FPS for stress directions at Redoubt during 1989-1990 and July 1991 are summarized in table 7. For convenience, we indicate the orientation of principal stress axes and the location in time and space of the different subsets analyzed. Inversion results that indicate homogeneity in the stress field are highlighted in bold.

Table 7. General Orientation of Stress Axes.

Time analysis			
Dec. 1989-Dec. 1990	σ_1	σ_2	σ_3
Phase I (Vent-clearing phase, first dome)	NW - SE	Z	NE-SW
Phase II (Second dome)	**NW - SE**	**NE - SW**	**Z**
Phase III (Repetitious dome)	WNW - ESE	NNE - SSW	Z
Phase IV (Post-eruption)	**WNW - ESE**	**NE -SW**	**Z**
Space Analysis			
July 1991	σ_1	σ_2	σ_3
Shallow events	NW - SE	Z	NE - SW
Deep events	**Z**	**NW - SE**	**NE - SW**
Southerly events	NW - SE	WNW	NE - SW
Northerly events	**Z**	**NE - SW**	**NW - SE**

7. Discussion

7.1. Changes in Stress with Time at Redoubt Volcano.

The application of the Gephart and Forsyth (1984) method of stress inversion from a population of FPS, and the Lu and Wyss (1995) cumulative misfit analysis to define boundaries between zones of different stress regime, have given results that suggest that the Redoubt area shows variations in stresses with time during 1989-1990. The curve of cumulative misfit vs. earthquake number by time (figure 10) shows changes in slope that define four segments identified at the 99% confidence level. Most of the events in each individual segment occur within the different stages of activity at Redoubt during the 1989-1990 eruptive sequence. Each of these stages was characterized by changes in type of seismicity, number and locations of earthquakes, and intensity of seismic signals (Power et al., 1994), as well as changes in the rates of growth and duration of lava domes (Miller, 1994). The termination of the post-eruption phase was determined arbitrarily as the first of October 1990, because seismic observations were not discussed in detail beyond that point (Power et al., 1994).

Earthquakes 1 to 15 define phase I in figure 10, and the inversion of FPS 1 to15 give a solution indicative of some degree of heterogeneity in the stress field. This phase includes mostly earthquakes that occurred following the major vent-clearing tephra

eruptions and growth of the first dome (A and B in figure 10). This temporal relationship suggests that these earthquakes are associated with stress readjustment due to the removal of magma and volatiles from depth (Power et al., 1994; Chouet et al., 1994; Lahr et al., 1994). Unfortunately, the small number of events suitable for computing FPS does not allow us to resolve better these time periods. The inversion result in this segment shows heterogeneity that may reflect the spatial and temporal separation of the earthquakes.

Earthquakes 16 to 67 define phase II in figure 10. These events occurred following the formation of the second lava dome at Redoubt after January 14, 1990. They may also represent readjustment of stress due to the movement of magma within the reservoir, located at depths between 6 and 10 km depth. The second dome had a life span of approximately 45 days, and observations of changes in its appearance during most of this time suggest that it grew steadily until early February (Miller, 1994). By inverting FPS of earthquakes within segment 2 of figure 10, we obtained a solution representative of homogeneity in the stress field (small average misfit), and we suggest that there is an association between the steady growth of the second dome and the homogeneous state of stress that dominated during its formation.

Earthquakes 68 to 178 define phase III in figure 10 and these events occurred after the beginning of the repetitious dome-building phase at Redoubt, during which a series of 12 domes were emplaced and subsequently destroyed. Again, the earthquakes may represent readjustment of stresses near the reservoir due to the movement of magma. The average duration of these domes was estimated to be 6 days and they were all smaller in volume

than the two earlier domes. This series of dome emplacement and destruction in relatively short periods may reflect instability (heterogeneity) of the stress field near the volcano. By using FPS within phase III we were not able to obtain a sample that could indicate homogeneity in the stress field. We suggest that this reflects a varying stress field near the magma reservoir during the time of repetitious dome-building at Redoubt.

A striking match is observed between the end of the repetitious dome-building stage and the beginning of phase 4 in the cumulative misfit vs. time curve (figure 10). Earthquakes 179 to 212 define phase 4, which occur during the post-eruption stage. This period was characterized by a continuous decline in the number of earthquakes, absence of swarms of long-period events, and episodes of low-level tremor accompanied by steam bursts. By inverting a subset of 19 events within this segment we obtained a solution that represents homogeneity in the stress field (table 2). This is consistent with observations at other volcanoes (Ui et al., 1974; Heleno da Silva et al., 1999) where a stabilization of the stress field has been suggested after the cessation of eruptive activity.

Finally, we note that there is an outstanding similarity between the general shape of figure 10 (this study) and figure 7 of Miller (1994), which shows the cumulative volume of andesitic lava extruded throughout the eruptive sequence (figure 24). This suggests that the state of stress is associated with volume and rate of lava erupted, the duration of each stage of activity, and the average duration of domes observed at Redoubt during 1990.

The above analysis indicates that differences in the state of stresses may exist at

Redoubt between periods of dome growth and dome destruction, and cessation of eruptive activity. We speculate that the complex activity that occurred at Redoubt during the repetitious dome-building phase may represent a variable and heterogeneous state of stress. Evidence for this comes from the results of inversion of FPS, which reflect heterogeneity in the stress field. We suggest that a stable and homogeneous stress field dominated during both the second dome-building phase and after the cessation of eruptive activity.

7.2. Changes of Stress as a Function of Space at Redoubt Volcano

We applied the methods of stress tensor inversion and cumulative misfit to identify spatial boundaries between regions of different stress near Redoubt volcano. The results suggest that the area around Redoubt is variable in stress with depth and distance to the volcano. For example, the inversion of 96 FPS from 1991 (figure 16) yielded a solution that is representative of a heterogeneous stress field. Division of the data set into subsets of FPS located above and below 6.4 km yielded inversion results that can indicate that the stress tensor acting below 6.4 km is different from that acting at shallower levels. This is supported by the identification of at least two segments in the cumulative misfit curve (earthquakes ordered by depth), and by the subsequent inversions of FPS in each segment (figures 15 and 16, table 4). For segment 2 in figure 9 (deeper events) the inversion results do not change, even when using only half of the FPS in the segment. Using 39

FPS, we found a solution that is stable, with a small misfit (4.5°) that suggests homogeneity in the stress field. We regard this solution as stable, reflecting a homogeneous stress field acting at depths between 6.4 and 9 km depth.

We also identified two distinct segments in the plot of cumulative misfit against earthquake number by latitude (figures 18-19). Segment 1, different from segment 2 at the 99% confidence level, comprises events south of 60.5° N that are distributed over a large area and have depths that vary between 0.9 and 11 km. Many of these events are shallow. Given these characteristics in their epicentral and hypocentral distribution, the stress model obtained from inverting such a heterogeneous data set was expected (table 6). Subdividing the data, we obtained a solution that has a smaller misfit (table 6) and is similar to that obtained for shallow events (table 4). If we regard the solution shown in figure 19b to be stable, but reflecting some degree of heterogeneity, we can postulate that shallow earthquakes south of 60.501° N occur in a stress regime that differs from that at deeper levels to the north. Segment 2 (in the curve of misfit vs. latitude, figure 18) includes events between 60.501° N and 60.553° N, the area sampled by most of the seismicity in the depth range 6 –10 km. Most earthquakes located in this zone occur where the postulated tabular magma source region exists, as described by Power et al., (1994) and Lahr et al., (1994). The inversion of FPS in this area gives results that indicate homogeneity in the stress field (see figures 19c-d). These results equal those obtained for deeper events (figure 16d). The stress field in this northerly region not only differs from the segment to the south, but also has a nearly-vertical maximum compressive stress.

From the results obtained by the stress inversions and cumulative misfit analysis, we observe that there are differences in the stress field with depth and latitude near Redoubt. In general, southerly and shallow events show a heterogeneous stress field with a near-horizontal σ_1 striking NW-SE, and a near-vertical σ_2; whereas northerly and deeper events are explained by a homogeneous stress field with a near-vertical σ_1 and a sub-horizontal σ_2 striking NW-SE.

Variations of stress in space have been reported at other volcanoes. Moran (2000) suggests that hydrothermal circulation deep within and beneath Mt. Rainier volcano (Cascades range) may be responsible for many shallow earthquakes occurring with very high dip angles, and a stress inversion revealed variability in the stress field in the Rainier area. Giampiccolo et al., (1999) found important differences in stress with depth in the Rainier area, in particular, events located in the Western Rainier Seismic Zone (WRSZ) (10-14 km depth) have a near vertical σ_3 direction, whereas other depth ranges in this area show a near-horizontal σ_3. The change in orientation of σ_3 in the WRSZ is speculated to be caused by the influence of the nearby Mount Rainier magmatic system (Giampiccolo et al., 1999). In our study, we found many events with normal faulting, and the stress inversion suggests a homogeneous stress field, acting in the deep cluster of events in the Redoubt area. This stress field is potentially different to that acting at shallower levels and nearer to the volcano.

Power et al. (1994) and Benz et al. (1996) suggested that the Redoubt magmatic system is composed of a deep magma source region connected to the surface by a thin

conduit. The temporal and spatial characteristics of the seismicity during and after the 1989–1990 eruptive sequence suggest that the deep source region is located between 6 – 10 km depth, and may be a tabular volume elongated to the north. This has been thought to be a magma reservoir that experienced changes caused by movement of magma during the eruption. In such an environment, VT earthquakes may occur when changes in magma pressure causes the dikes to expand in the direction of σ_3 or contract in the direction of σ_1, creating a swarm of earthquakes caused by sliding of multiple faults surrounding the dikes and connecting the tips of dikes and cracks (Hill, 1977). In some cases the maximum compressive stress would be oriented vertically, and the dikes (and therefore, the adjoining faults connecting them) would be oriented according to the maximum stress in the horizontal plane, σ_2.

The apparent differences in orientation of σ_1 and σ_2 between shallow and deep events at Redoubt may be caused by differences in the pore pressure with depth beneath the volcano. Evidence for this at other volcanoes comes from results of *b*-value (the frequency-magnitude distribution) studies at volcanic areas such as Mount St. Helens, Washington, and Spurr, Alaska (Wiemer and McNutt, 1997). At Mount St. Helens, two volumes of anomalously high *b*-values (more small earthquakes) coincide with a suggested shallow magma reservoir or zone of vesiculation and a deeper magma reservoir. The shallow anomaly at depths of 2.6-3.6 km is associated with a zone altered by vesiculation and disruption of ascending magma (Pallister et al., 1992; Chadwick et al., 1988) which causes the rocks to fracture and increase the *b*-values. Thus high b-

values are associated with differences in fluid pressure at depth. Alternatively, high temperatures, lower effective stress, and/or higher heterogeneity may also cause anomalously high *b*-values (Wiemer and McNutt, 1997).

7.3. Rotation of Stress Axes at Redoubt and Estimation of Absolute Levels of Stress

In this section we focus on earthquakes located between 6-9 km depth. Shallow earthquakes are excluded because they are observed mostly in 1991. In table 7 we see that throughout the eruptive sequence, σ_1 was near-horizontal and striking SE-NW and σ_3 was near-vertical. In contrast, the inversion results during July 1991 show that events in the depth range of 6-9 km are explained by a homogeneous stress tensor with near-vertical σ_1 and either near-horizontal σ_2 or σ_3 oriented SE-NW. Assuming that immediately after the end of the eruptive sequence the state of stress near the volcano was as shown in figure 11g (phase IV), we speculate that their positions were switched by July 1991 as shown in figure 16d (deep and northerly events).

From the rotation of principal stress axes between 1990 and July 1991, we can estimate the absolute and relative values of stresses near Redoubt. We assume an invariable tectonic stress during 1990-1991 and that a vertical σ_1 represents the stress

caused only by the overburden of a column of rock. Let σ_1(A), σ_2(A), and σ_3(A) be the values of σ_1, σ_2, and σ_3 in June 1990, immediately after the end of the eruption sequence (figure 11g, stage A in figures 21 and 22), and let σ_1(B), σ_2(B), and σ_3(B) be the values of σ_1, σ_2, and σ_3 during July 1991 (figure 16d, stage B in figures 21 and 22). The vertical load at 7 km depth is approximately:

Vertical load = rgh = (2,650 kg.m^{-3}) x (9.8 m.s^{-2}) x (7000 m) = 181.8 MPa = 1818 bar,

then, σ_1(B) = 1818 bar, therefore σ_2(B) < 1818 bar, and σ_3(B) << 1818 bar.

By the end of the eruptions the state of stress was represented by a nearly-vertical σ_3, which represents extension or tensional stresses acting vertically. We also know that the strength of rocks in tension is about 50 bar (Locker, 1995), therefore, to produce slip in this conditions, rocks must overcome both the overburden and the tensional strength, which gives: σ_3(A) = (1818+50) bar, and since σ_3(A)<σ_2(A)<σ_1(A), we can write: σ_2(A) = (1818+50+Δs) bar, and: σ_1(A) = (1818+50+Δs+δs) bar. Here Δs and δs are quantities that we cannot determine, and represent the differences in stress level between the principal axes. The observed changes in directions of stresses between 1990 and 1991 suggest that the values of σ_1, σ_2, and σ_3 are similar to each other and are in the range 1818 bar to (1818+50+Δs+δs) bar.

We interpret this exchange of stress axes between the period immediately following the 1989- 1990 eruptive sequence and July 1991 as caused by the expansion and contraction of the magma body that is thought to lie north of Redoubt's summit (Power et al., 1994; Benz et al., 1996). Evidence for this is the observation that throughout the

eruptive sequence reverse and strike-slip faulting dominated, whereas during July 1991 normal faulting was dominant. Also, assuming that the earthquakes during July 1991 represent the activity during repose time (the period between eruptions), they may represent the state of stress during the pre-eruptive period (stage C in figure 22), from which there is not sufficient data suitable for stress inversion analyses. Finally, we suggest that a change in the relative values of horizontal stresses, from the pre-eruptive period to the end of the eruption, is better explained by the expansion and contraction of a magma body composed of dikes and sills with different orientations, as opposed to a single vertical dike. To visualize this, we constructed figures 21 and 22, plotting the evolution of absolute and relative levels of stress during 1989-1991 on a fixed reference frame. The lower part of the graph shows a simplification of a magma reservoir in which a point located near the magma reservoir (a dike, or a system of dikes and sills) would feel changes in stresses related to expansion and contraction of the reservoir. The sketch in the lower part of figure 21 illustrates an expanding and contracting vertical dike. We believe that such movements cannot totally explain the observed stress changes in the NW-SE direction, whereas a less geometrically uniform system of dikes can account for the changes in all horizontal directions (figure 22).

7.4. Deviation of Stresses at Redoubt from the Expected Regional Field Resulting from Plate Collision.

We want to determine whether the orientation of principal stress axes obtained during July 1991 differs from the regional stress field acting around Redoubt. Nakamura (1977) proposed a method for determining the orientation of average tectonic stress using surface features that indicate radial dike patterns of volcanoes. The method is based on the identification of dikes and eruption fissures from the distribution of flank craters near volcanoes. According to his assumption, the distribution of flank craters will be elongated in the direction of the maximum horizontal compression of the regional stress, and dikes will expand in a direction parallel to the minimum horizontal compression. The method has been tested at many volcanoes around the world (Nakamura et al., 1977), and in most places the orientations of flank craters are aligned with the expected regional horizontal compressive stress, due to plate convergence, including Iliamna and Spurr volcanoes, where alignment of flank cones were found to be in a NW direction (Nakamura et al., 1977). They concluded that flank craters align in the direction of plate collision.

From inversion of FPS of regional earthquakes in the vicinity of Mt. Spurr, Alaska, Jolly et al., (1994) found that the regional events are explained by a stress tensor with a near-horizontal σ_1 striking SE-NW (azimuth = 330°, plunge = 30°) and a near-horizontal σ_3 striking SW-NE (azimuth = 221°, plunge = 39°). At Redoubt volcano, we found that during the 1989-1990 eruptive sequence, the orientation of principal stress axes agrees

with the expected orientation in the area, assuming that the regional stress field near Spurr and Iliamna volcanoes holds for the region near Redoubt (figure 11). During July 1991, however, the inversion results indicate a significant departure from the expected values, because subsets of events in the depth range 6-9 km are explained by homogeneous stress tensors with a near-vertical σ_1 and a near-horizontal σ_2 or σ_3. We suggest that this deviation is caused by decrease in pressure within the deeper portions of a magma reservoir located N-NW of the summit during July 1991. Similar results have been found at or near other volcanoes, although different processes have been suggested to cause the deviation of stress directions (Barker and Malone, 1991; Moran, 1994, 2000; Giampicolo et al., 1999). Figures 23a-b show, schematically, the orientation of principal stresses near Redoubt, both locally, and compared to the regional setting.

8. Conclusions

We used the method of Gephart and Forsyth (1984) to find the best-fitting stress tensor for groups of fault plane solutions near Redoubt volcano. We also applied the cumulative misfit method (Lu and Wyss, 1995) to identify segments with different slope in cumulative misfit plots against earthquake number ordered by time, depth, and latitude. We identified at least four phases, different at the 99% confidence level, in the cumulative misfit vs. time curve. There is an association between these phases and the stages of activity in the 1989-1990 eruptive sequence at Redoubt volcano, indicating that the stress near the volcano changes with eruptive style. We suggest that differences in state of stress may exist at Redoubt between periods of dome growth and destruction and cessation of eruptive activity. The varying activity that occurred at Redoubt during the dome-building stage may represent a variable and heterogeneous state of stress. Evidence for this comes from the results of inversions of FPS, which reflect heterogeneities in the stress field. A stable and homogeneous stress field dominates during the second dome building stage and after the cessation of eruptive activity. The evidence for this is the inversion of subsets of FPS, which gave solutions with low average misfits.

We identified 2 segments, different at the 99% confidence level, in each of the cumulative misfit-depth and the cumulative misfit-latitude curves. Inversion of FPS within individual segments show that events in the range 6-9 km are explained by a

homogeneous stress tensor with a near- vertical σ_1, a near-horizontal σ_2 striking SE-NW, and a near-horizontal σ_3 striking perpendicular to the direction of plate convergence. We suggest that changes in pressure of the magma reservoir underneath Redoubt may have caused the earthquakes around this weakened, possibly semi-emptied magma storage zone. Earthquakes north of 60.5° N are explained by a stress tensor that is similar to that for earthquakes in the depth range 6-9 km.

Differences in stress orientation were found between the period following the cessation of eruptive activity and July 1991. We hypothesize that this rotation in stress directions indicates values of absolute stress level for σ_1, σ_2, and σ_3 that are similar to each other, with values in the range 1818 to (1818+50+Δs+δs) bar. Their changes in position may reflect expansion and contraction of the magma reservoir located underneath Redoubt.

The inversion results show that earthquakes near Redoubt during July 1991 are explained by a stress tensor that deviates significantly from the expected regional field resulting from plate collision, with a near-vertical σ_1, and near-horizontal σ_2 and σ_3 striking SE-NW and SW-NE, respectively.

9. Suggestions for Future Research

1. We need to analyze regional earthquakes and invert for stress directions to see if they differ from the directions found near Redoubt, and to have a better understanding of regional versus local stresses. Several workers have documented apparent variations of stress near volcanoes, and also deviations from the tectonic stress (Ui et al., 1977; Barker and Malone, 1991; Moran, 1994; Jolly et al., 1994; Giampiccolo et al., 1999; Moran et al., 2000). For a group of earthquakes near Redoubt volcano in July 1991 we found indications of deviation from the tectonic stress field.

2. More research is needed to know if the apparent deviations of stress near Redoubt are common among monitored volcanoes in Alaska.The stress field at most Alaskan volcanoes is poorly known. McNutt and Sánchez (2000) studied composite focal mechanisms for earthquakes at Dutton, Pavlof, Akutan, and Makushin volcanoes and found that at Pavlof, Akutan, and Makushin the orientations of the P-axes deviate from the direction of plate convergence (see Appendix B). We point out, however, that the network configurations and density of stations could be a shortcoming when computing FPS. More stations around the volcanoes are needed to ensure better data quality and sufficient information to constrain fault plane solutions.

3. Little is known on deformation and stress changes caused by intrusions at Alaskan volcanoes. To improve our understanding of these processes, we suggest the study of

stress changes due to instrusions of simple geometrical shape using the Mogi model. Also, we encourage the study and modeling of stress changes caused by an opening dike, as well as the use of GPS (Global Positioning System) surveys around active volcanoes.

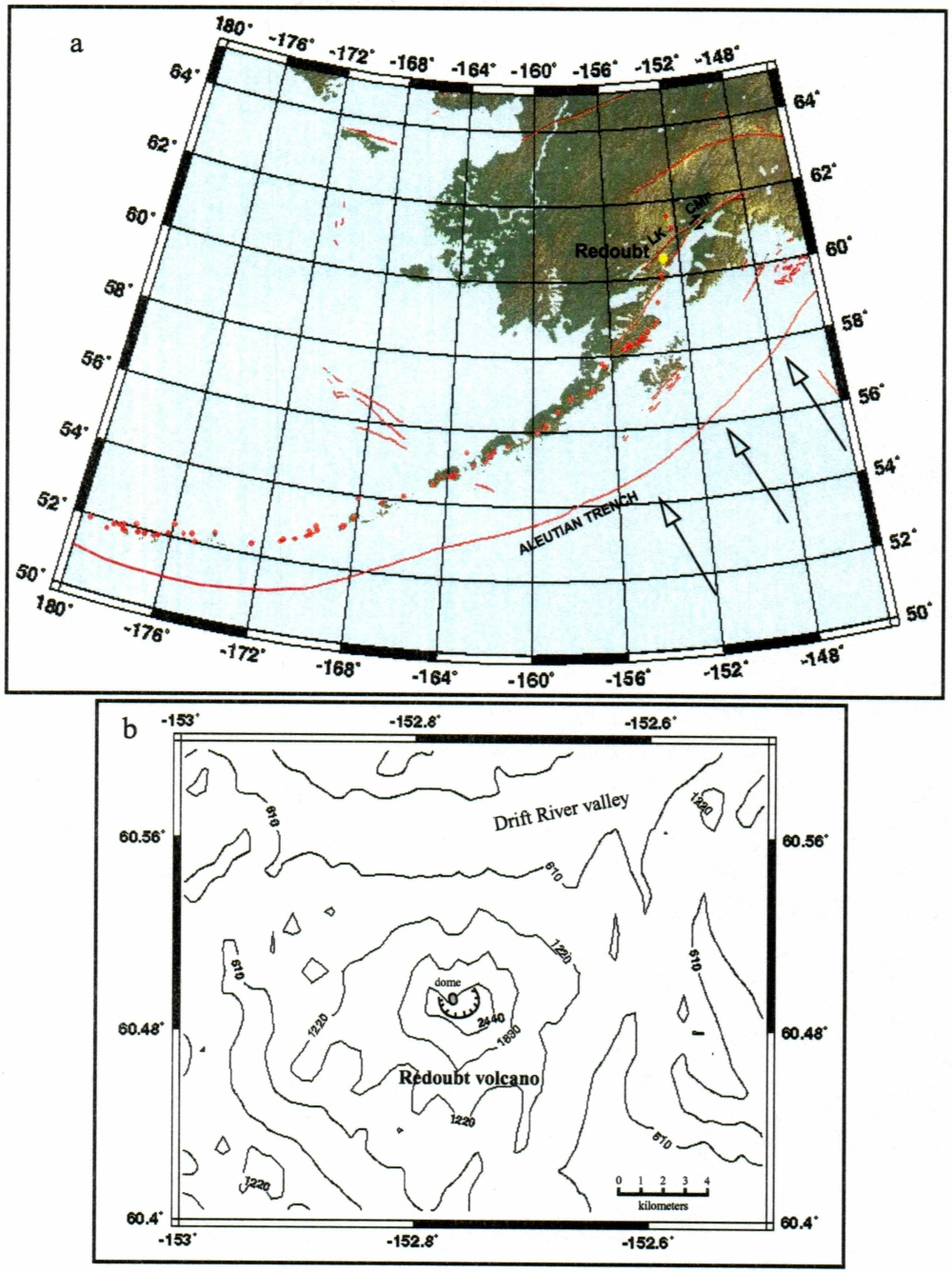

Figure 1. Location Maps of Redoubt Volcano. (a) Regional map with location of Redoubt volcano. Arrows show the direction of plate convergence. Yellow dot marks Redoubt volcano, red dots mark other volcanoes, red lines show main faults. CMF = Castle Mountain Fault, LK= Lake Clark Fault. (b) Local map showing topography in the Redoubt area. Contours are in meters. The horseshoe-shaped feature at the center marks the crater. Shaded oval marks the location of the vent where domes were extruded during 1989-1990.

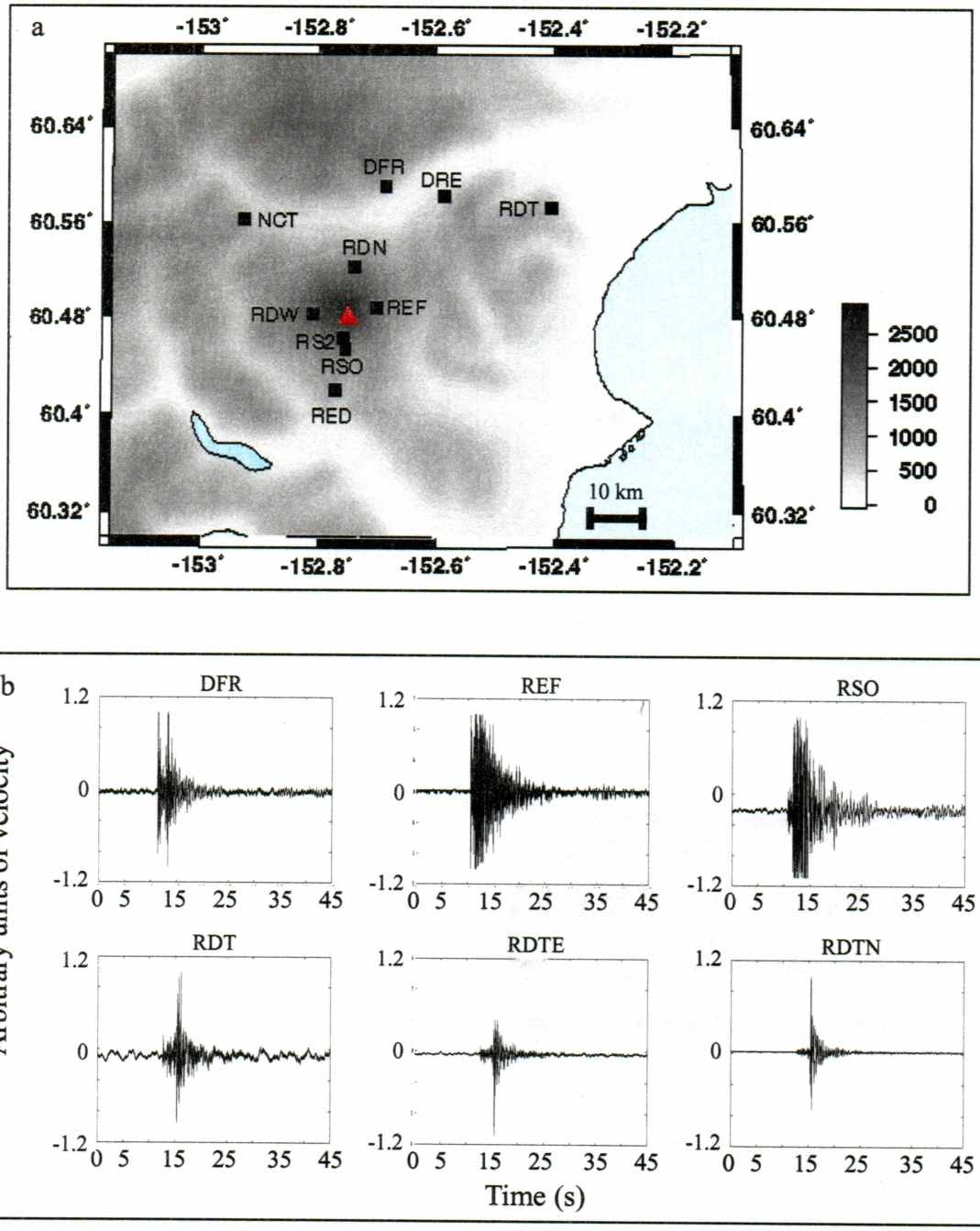

Figure 2. Location of AVO Stations and Example of Record. (a) Location map of AVO permanent network of seismographs. Red triangle marks the summit of Redoubt volcano. Solid squares mark the seismograph stations. Shading contours are in meters. (b) Vertical-component records of a typical VT earthquake that occurred on 03/24/90 at 21:12, recorded by AVO network. *ML*= 0.6; *Z* = 7.24 km. Horizontal scale in time (s). Vertical scale in arbitrary units of velocity.

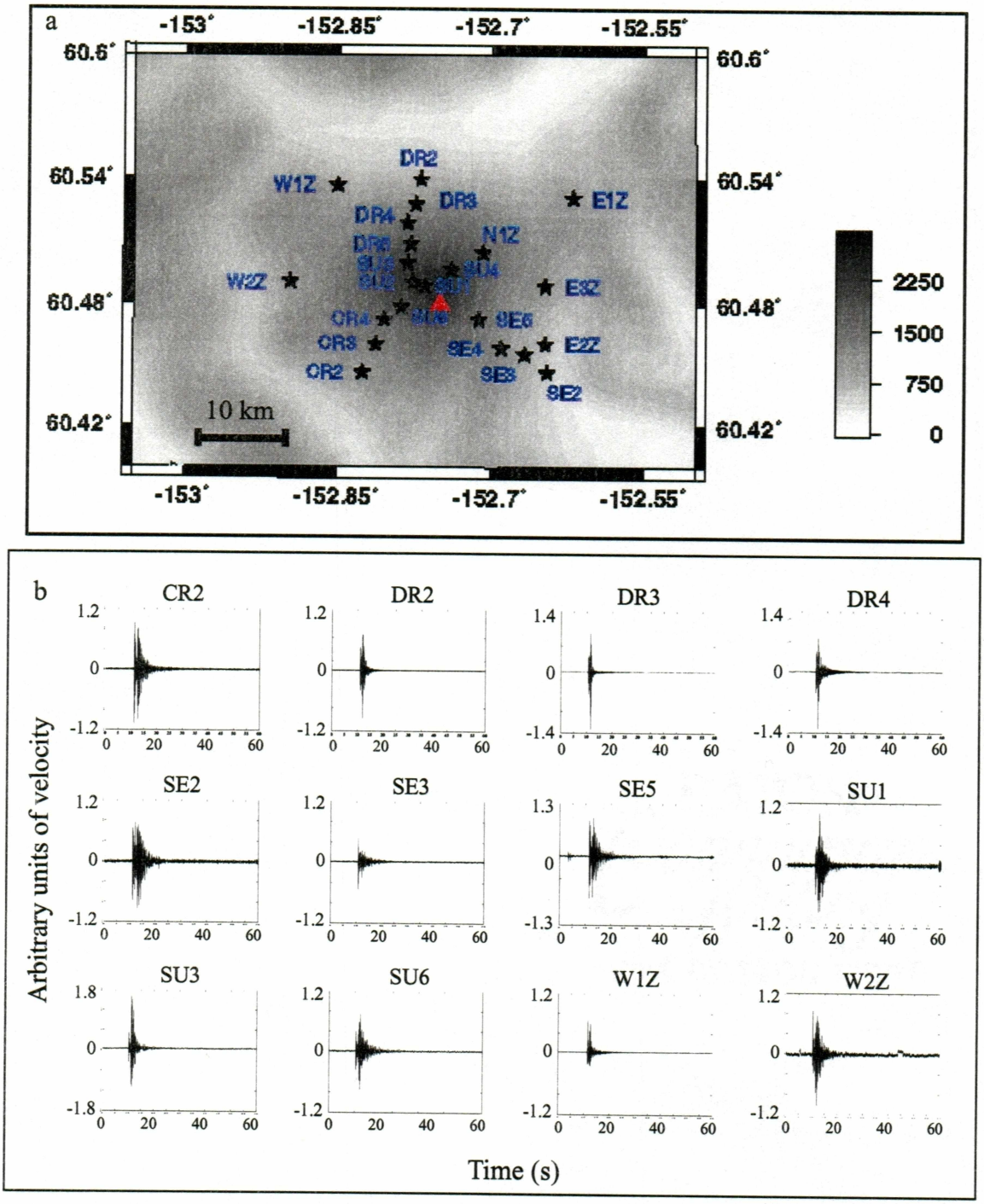

Figure 3. Location of PASSCAL Stations and Example of Record. (a) Location of PASSCAL temporary seismographs deployed during July 1991. Red triangle marks the summit of Redoubt volcano. Stars mark the seismograph stations. Other conventions as in figure 2a. (b) Vertical-component record of a typical VT earthquake that occurred on 07/17/91 at 14:43. $ML = 0.9$; $Z = 4.15$ km. Conventions as in figure 2b.

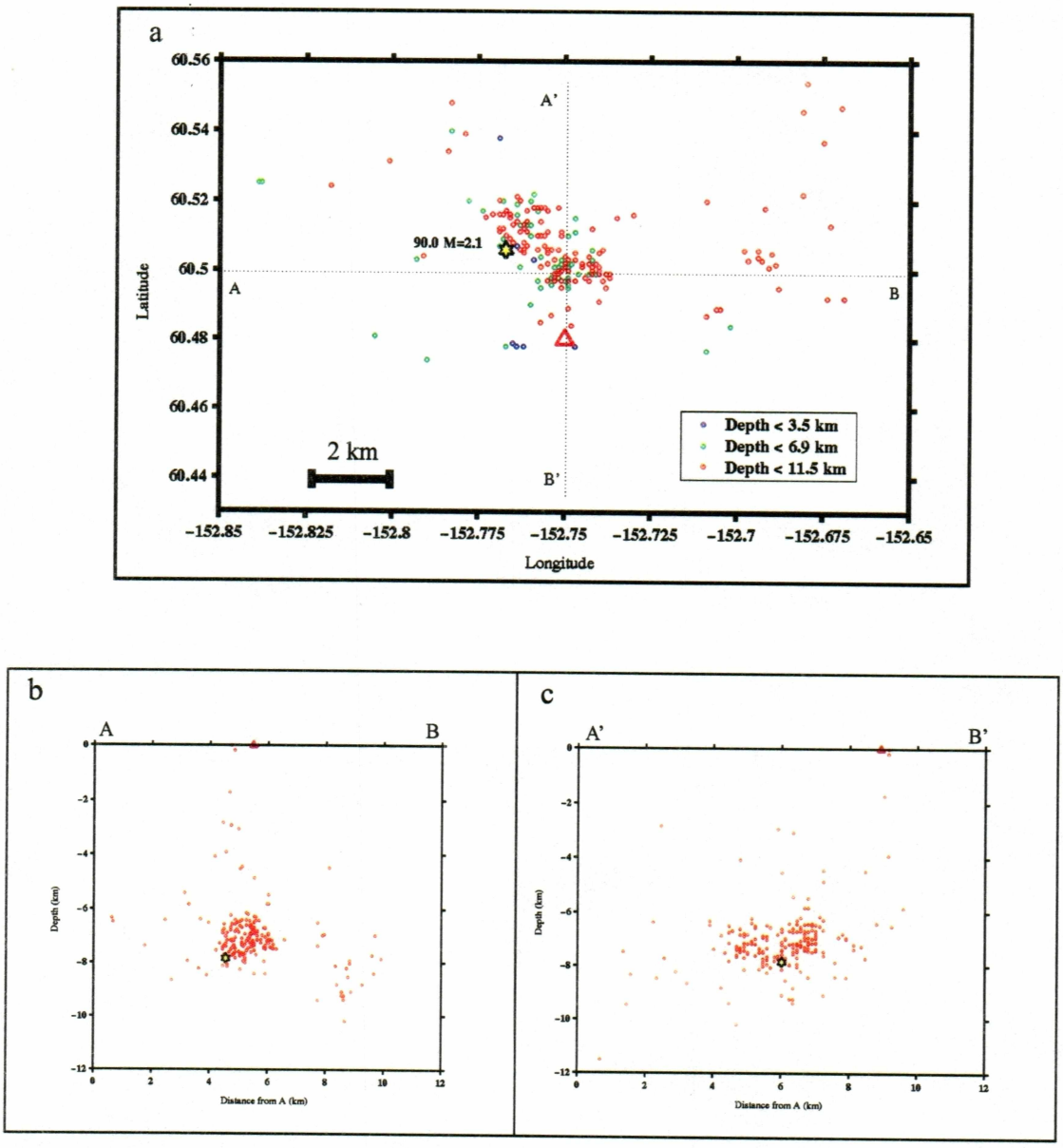

Figure 4. Location of Earthquakes During 1989-1990. (a) Locations of epicenters of earthquakes used for the analysis of variation of stress with time at Redoubt volcano during 1989-1990. Redoubt is marked by the red triangle. Yellow star marks the largest earthquake in the data set (see text for details). Zero depth datum is the summit crater floor, which is 2.3 km above sea level. Epicenters are color-coded by depth as follows: blue = $Z < 3.5$ km; green = $Z < 6.9$ km; red = $Z < 11.5$ km. (b) E-W cross-section (A-B in figure 4a) of hypocenters. Other conventions as in figure 4a. (c) N-S cross-section (A'-B' in figure 4a) of hypocenters. Other Conventions as in figure 4b.

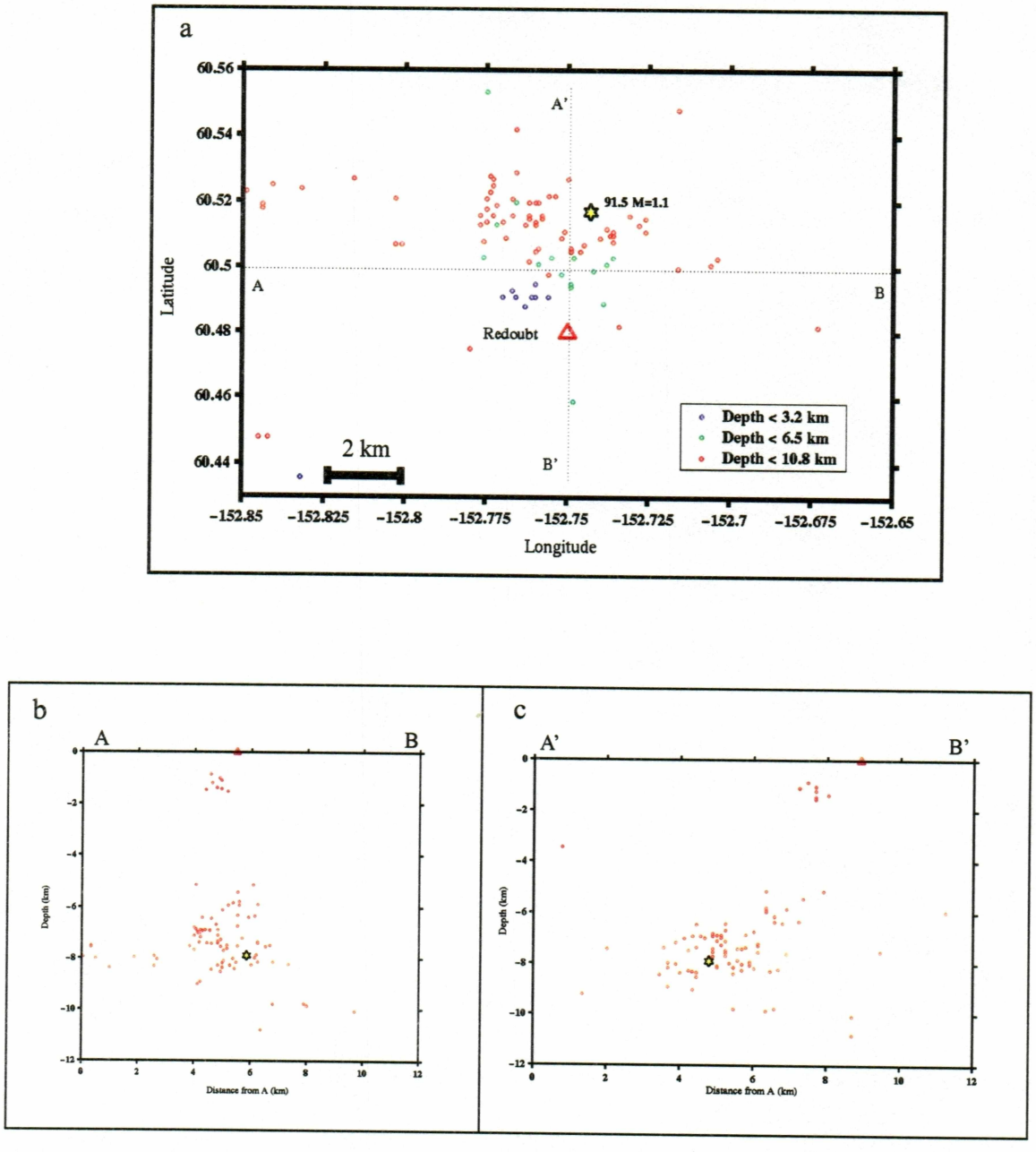

Figure 5. Location of Earthquakes During July 1991. (a) Locations of epicenters of earthquakes used for the analysis of variation of stress with depth and latitude during July 1991. Epicenters are color-coded by depth as follows: Blue = $Z < 3.2$ km; green = $Z < 6.5$ km; red = $Z < 10.8$ km. Other conventions as in figure 4a. (b) E-W cross-section (A-B in figure 5a) of hypocenters. Other conventions as in figure 5a. (c) N-S cross-section (A'-B' in figure 5a) of hypocenters. Other conventions as in figure 5b.

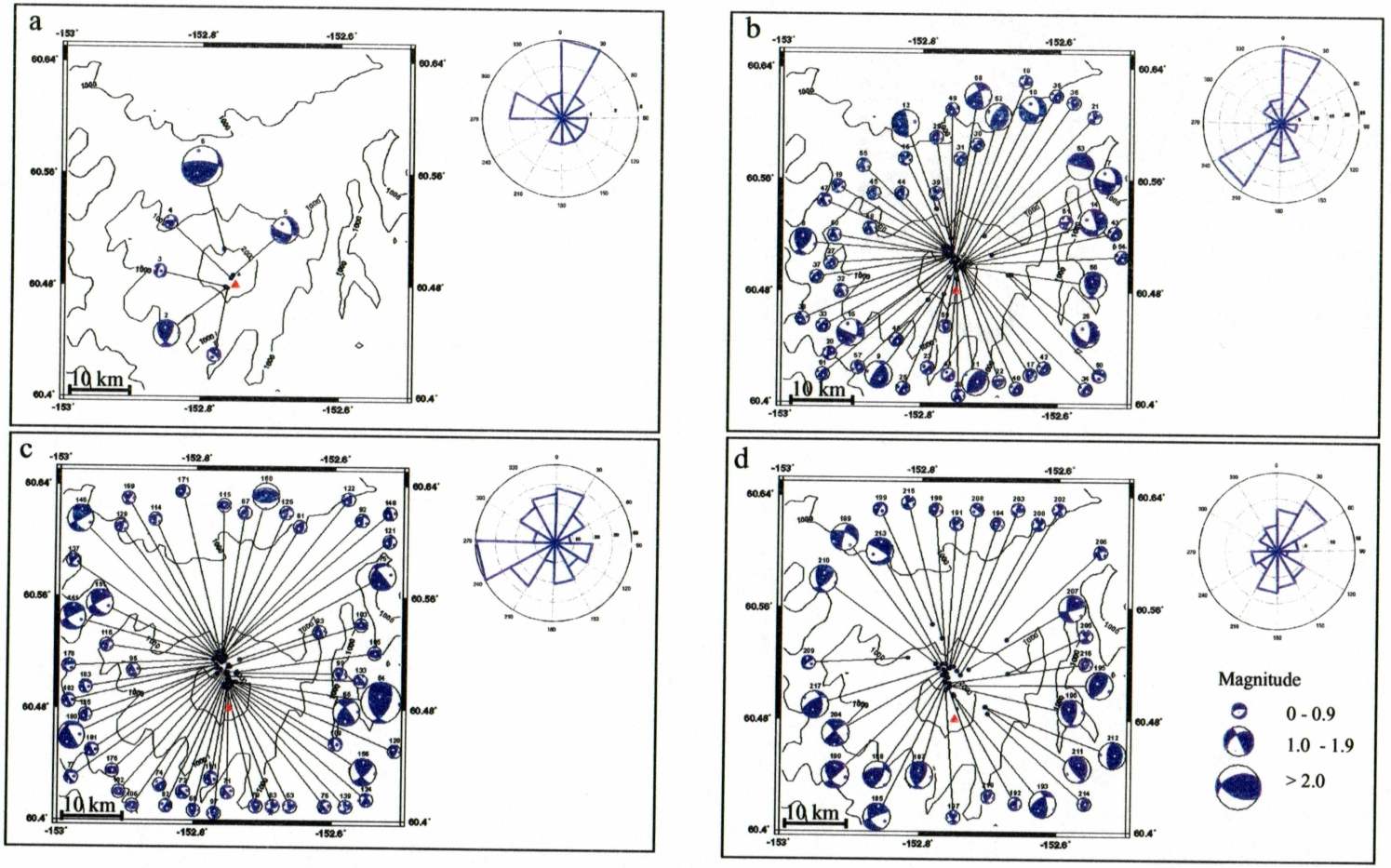

Figure 6. Fault Plane Solutions at Redoubt During 1989-1990. (a) Vent-clearing and first dome-building stage. (b) Second dome-building stage. (c) Repetitious dome-building stage. (d) Post- eruption stage. Lower hemisphere equal-area projections are used. Dilatational quadrants are white, compressional quadrants are blue. P and T-axes are blue and white dots, respectively. Redoubt is marked by a solid red triangle. Contours are in meters. Rose diagrams show the orientation of nodal planes.

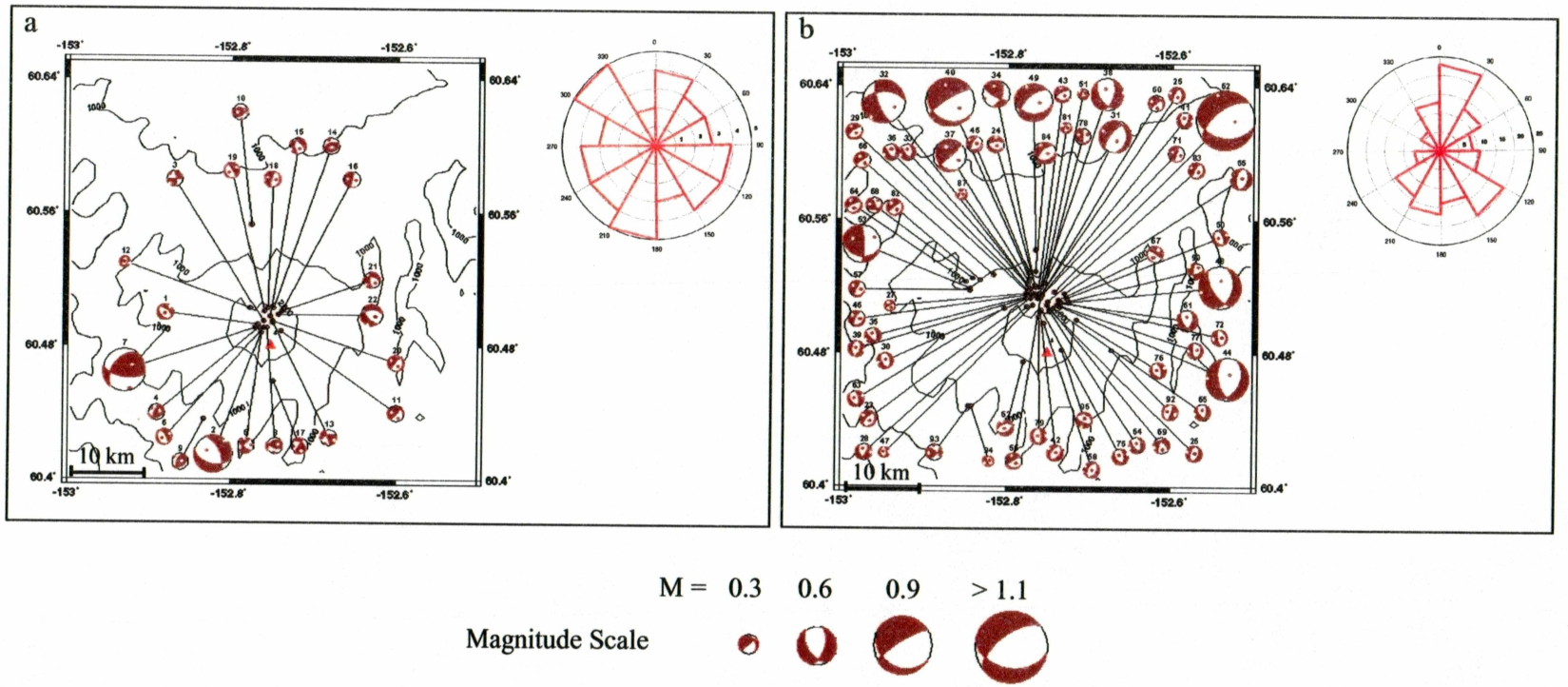

Figure 7. Fault Plane Solutions at Redoubt During July 1991. (a) Events between 0 and 6.4 km depth. (b) Events between 6.4 and 11 km depth. Lower hemisphere equal-area projections are used. Dilatational quadrants are white, compressional quadrants are red. P and T-axes are red and white dots, respectively. Other conventions as in figure 6a.

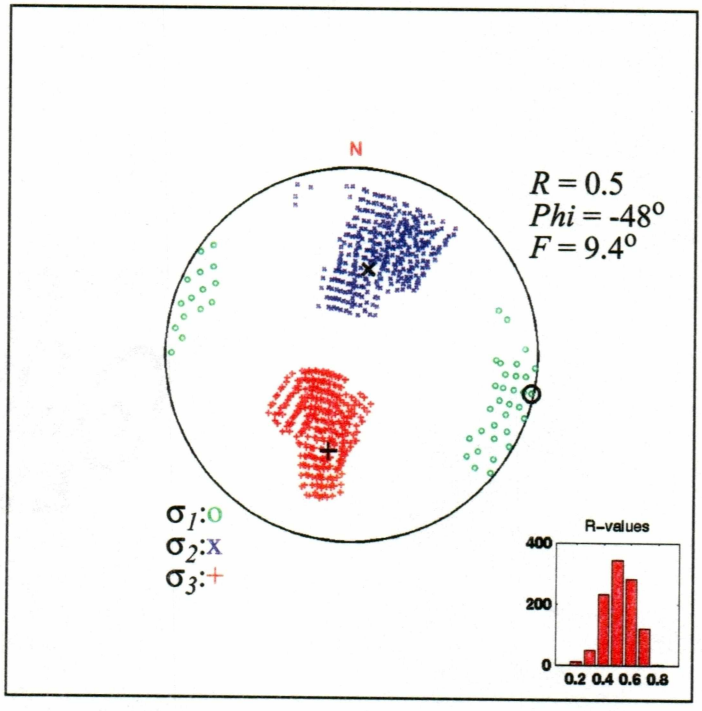

Figure 8. Principal Stress Directions Estimated From 212 FPS. 1989-1990.
Stereographic projection of the principal stress directions estimated by inversion of 212 FPS during 1989 - 1990. The range of orientations within the 95% confidence limits are shown, as well as computed values of R, ϕ, and F. The histogram shows the distribution of R values. Green circles, and blue and red crosses, are range of possible orientations for the direction of the maximum σ_1, intermediate σ_2, and minimum σ_3 principal stress axes. Black circle, and crosses are the directions of stress for the best fitting model.

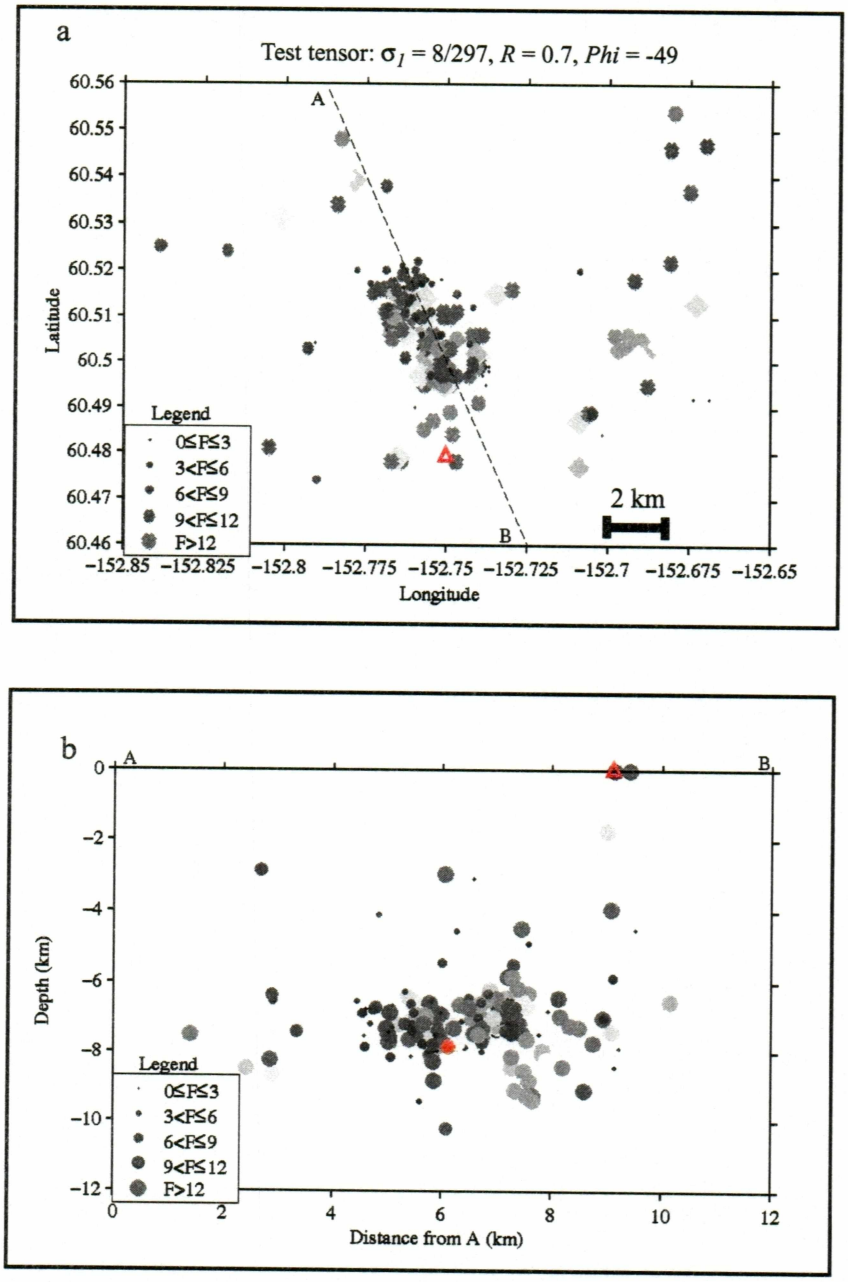

Figure 9. Individual Misfits of FPS During 1989-1990. (a) Map of individual misfits of FPS during 1989-1990. The color-coded misfit of each FPS with respect to a test tensor is plotted. Small and black symbols are small misfits, large and light grey symbols are large misfits. Redoubt is marked by a red triangle. Dotted line shows the orientation of cross-section. (b) Cross-section of misfits (A-B in figure 9a). Red star marks the largest earthquake. Other conventions as in figure 9a.

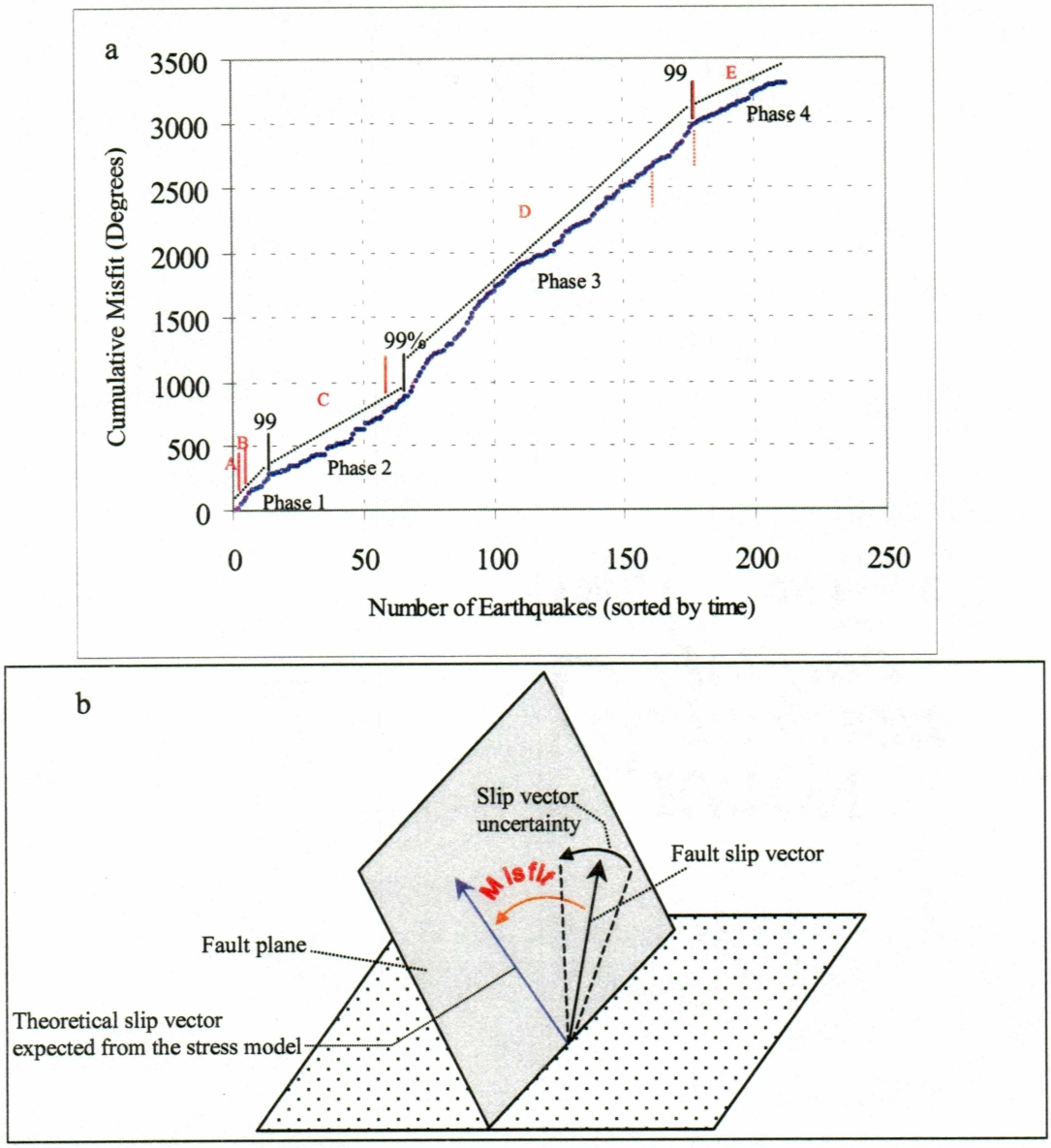

Figure 10. Cumulative Misfit vs. Time during 1989-1990. (a) Cumulative misfit vs. number of earthquakes, ordered by time, for earthquakes during 1989-1990. Black dotted lines show the phases proposed. Vertical black lines show the event were the change in slope occurs. Capital letters denote the stages of activity at Redoubt as described by Power et al. (1994). A: vent-clearing stage, from 12/14/89 to 12/19/89; B: first dome-building stage, from 12/19/89 to 1/2/90; C: second dome-building stage, from 1/2/90 to 2/15/90; D: repetitious dome-building stage, from 2/15/90 to 6/15/90; E: post-eruption stage, from 6/15/90 to 10/1/90. Vertical red lines show the limits between stages. Vertical dotted red lines show the estimated time of growth for dome number 14, which was not destroyed and signaled the end of the eruptive activity. (b) Schematic representation of the misfit between a FPS and the geometry expected from a stress model.

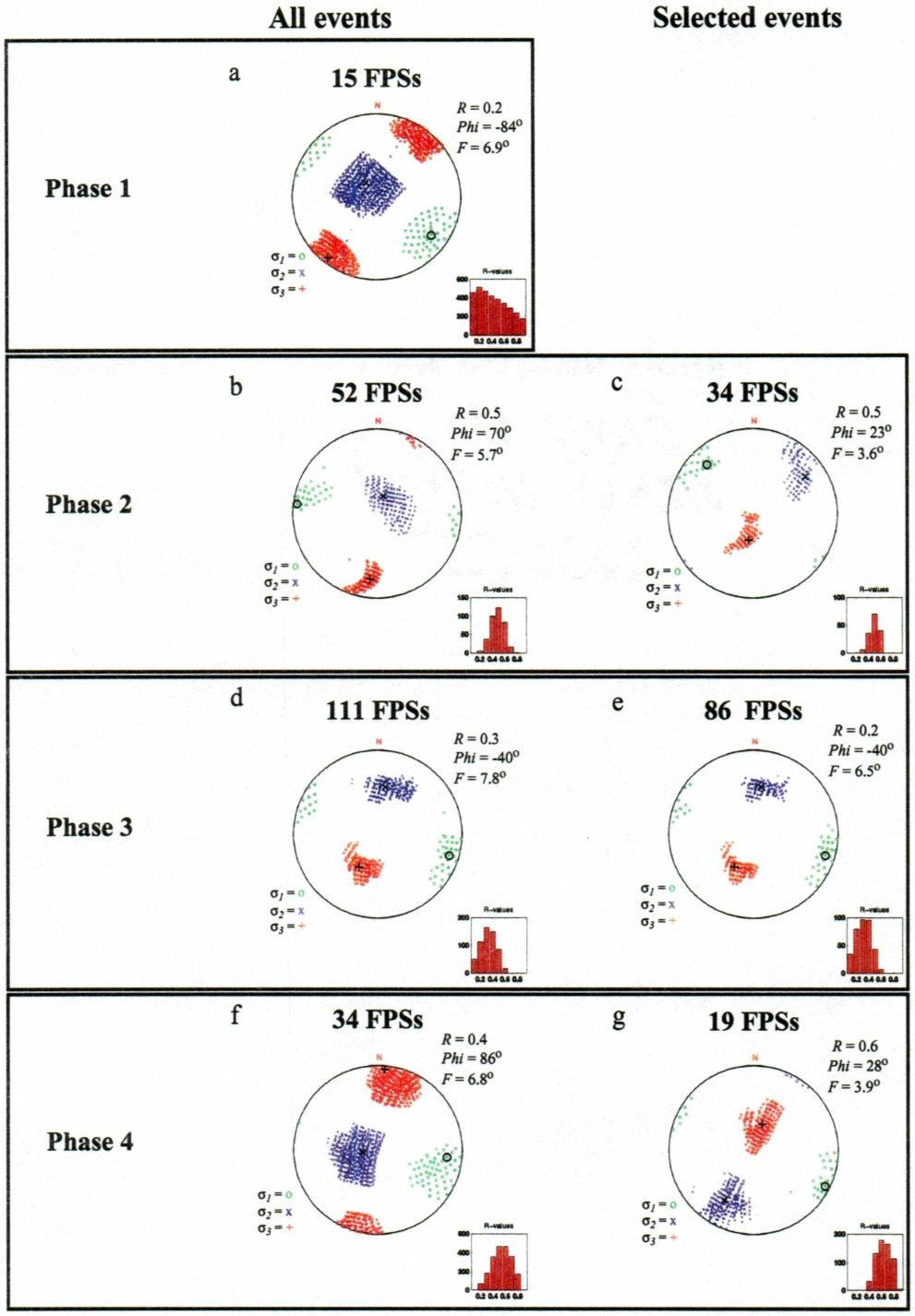

Figures 11a-g. Principal Stress Directions as a Function of Time, 1989-1990. Stereographic projections of principal stress, estimated by inversions of FPS as a function of time. Data for the period 1989-1990. Stress directions obtained by inverting all FPS (a, b, d, f) and subsets within each phase (c, e, g) are shown. "Phase" refers to individual segments identified in figure 10. Conventions as in figure 8.

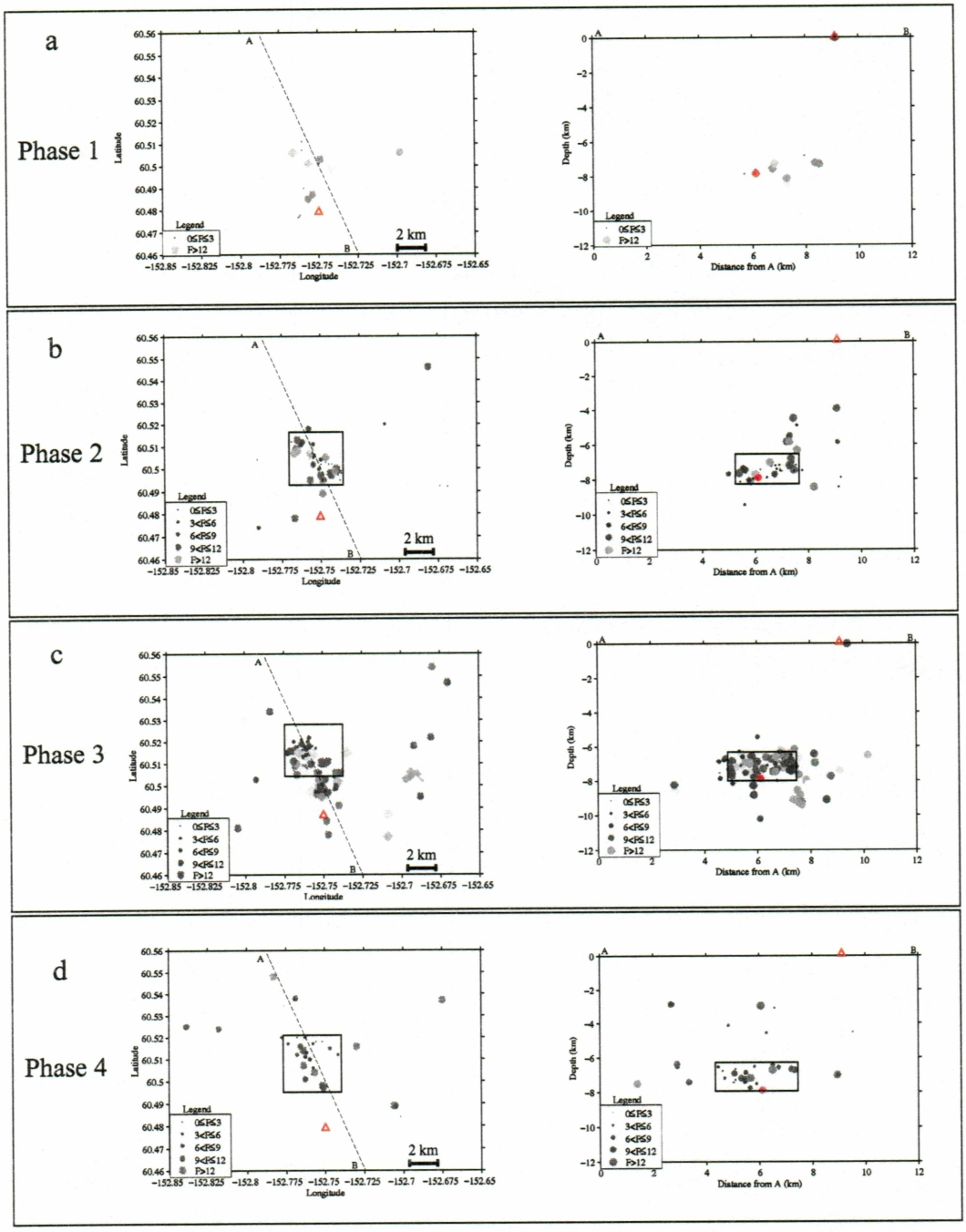

Figures 12. Maps of Individual Misfits for Each Phase Identified in Figure 10. (a-d) Maps and cross-sections of misfits, during 1989-1990, for events within individual segments of figure 10. Test tensor as in figure 9. Boxes show the regions where subsets of FPS were selected. Other conventions as in figures 9a and 9b.

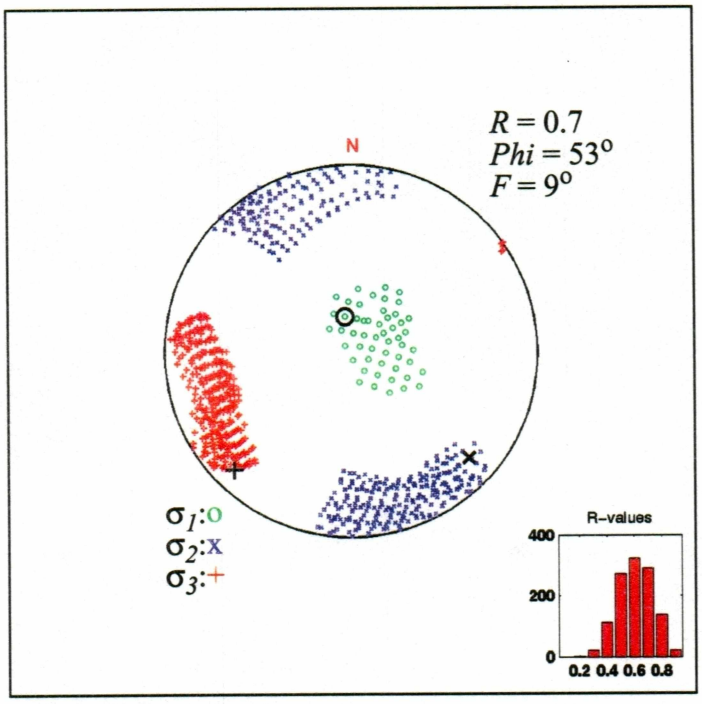

Figure 13. Principal Stress Directions Estimated From 96 FPS, July 1991. Stereographic projection of the principal stress directions estimated by inversion of 96 FPS during July 1991. Conventions as in figure 8.

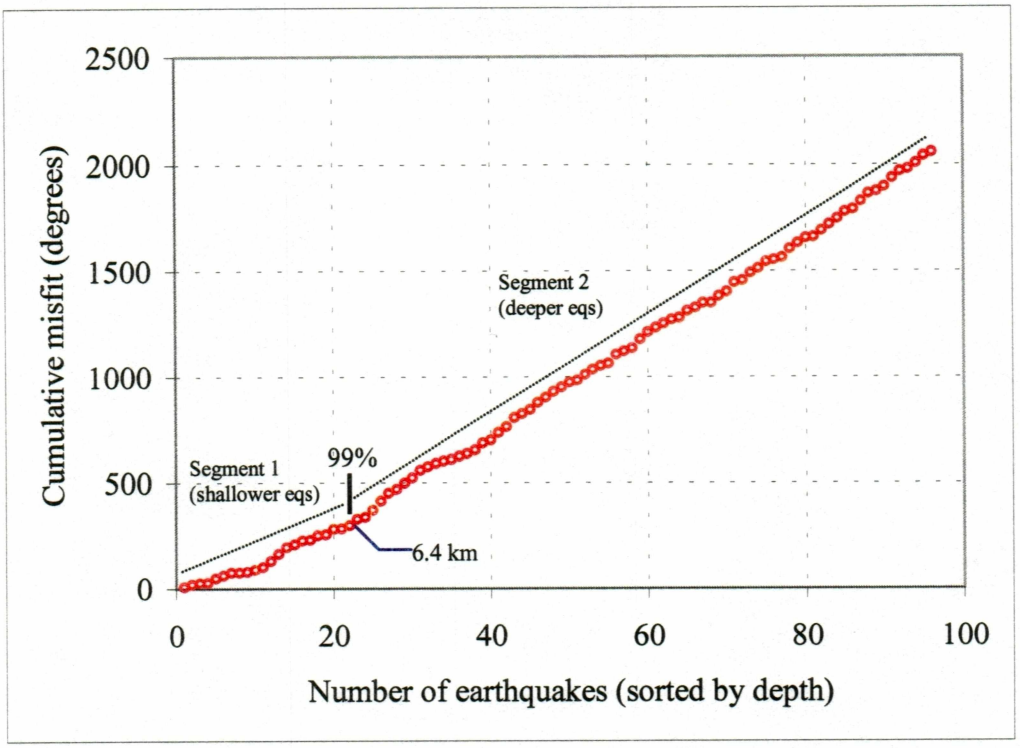

Figure 15. Cumulative Misfit vs. Depth During July 1991. Cumulative misfit vs. number of earthquakes, ordered by depth, for earthquakes during July 1991. Black dotted lines show the segments proposed. Vertical black line shows the event were the change in slope occurs. For information on the nature of errors involved in this plot see figure 10b.

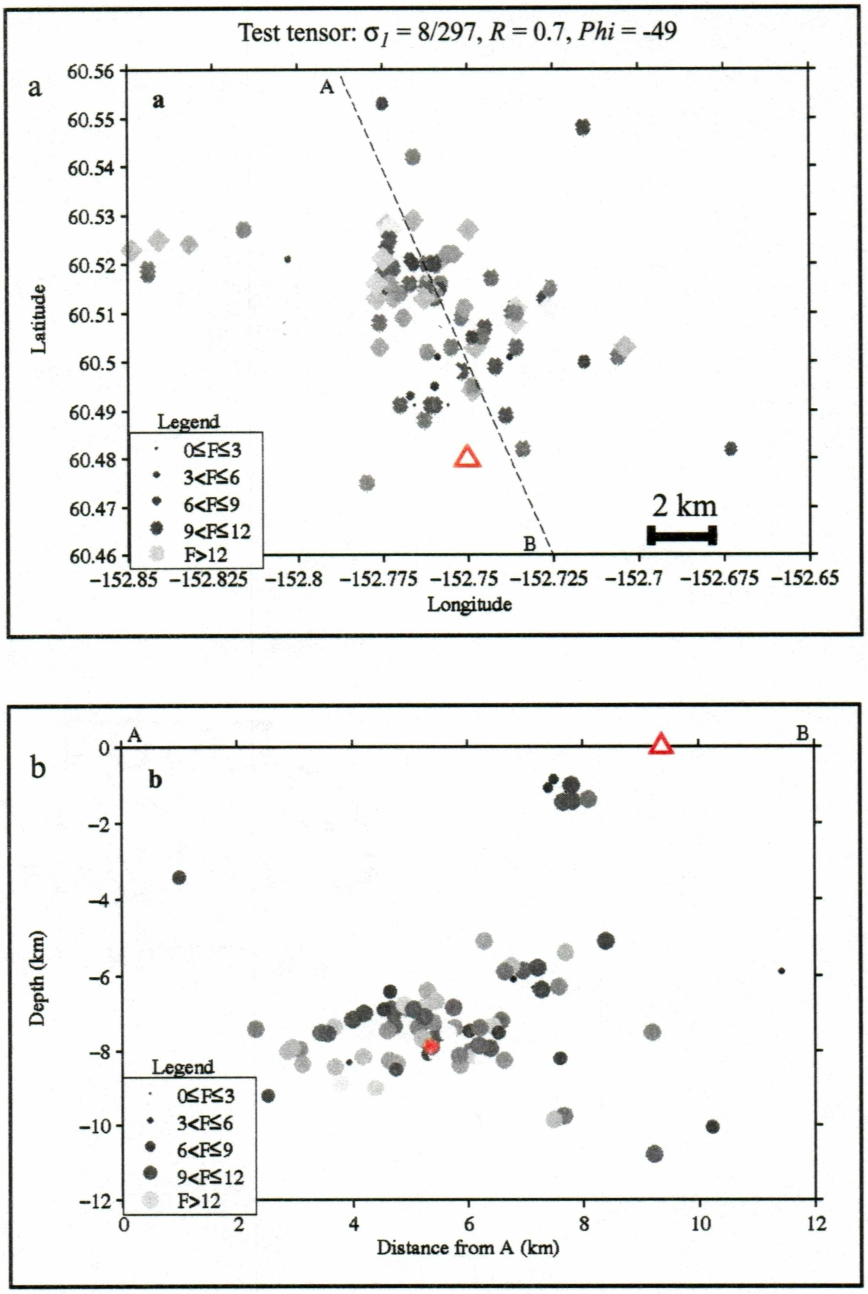

Figures 14. Individual Misfits of FPS During July 1991. (a) Map and (b) cross-section of individual misfits of FPS during July 1991. Conventions as in figures 9a-b

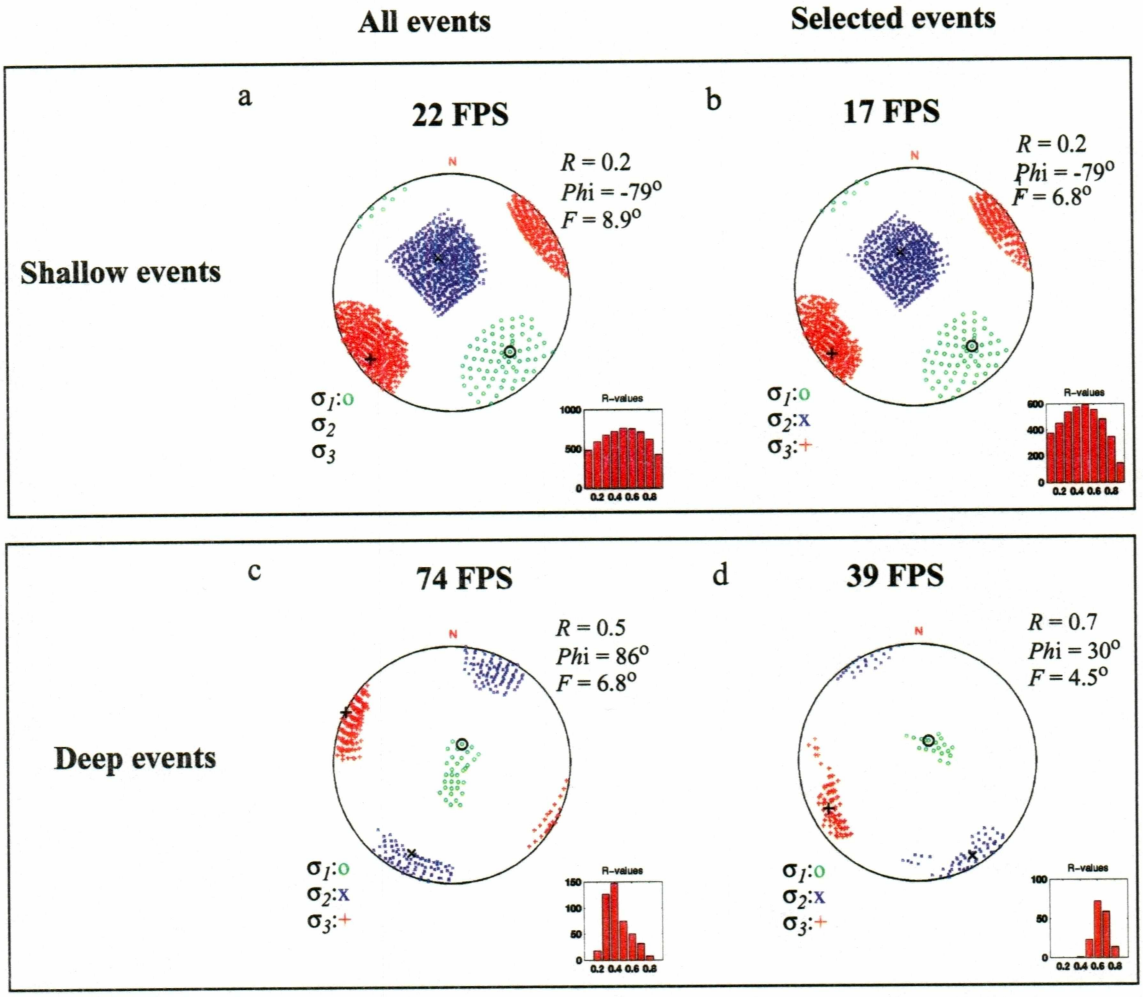

Figures 16. Principal Stress Directions as a Function of Depth, July 1991.
(a-d) Stereographic projections of principal stress directions, during July 1991, estimated by inversions of FPS within individual segments of figure 15. Stress directions obtained by inverting all FPS (a, c) and subsets within each segment (b, d) are shown. Conventions as in figure 8.

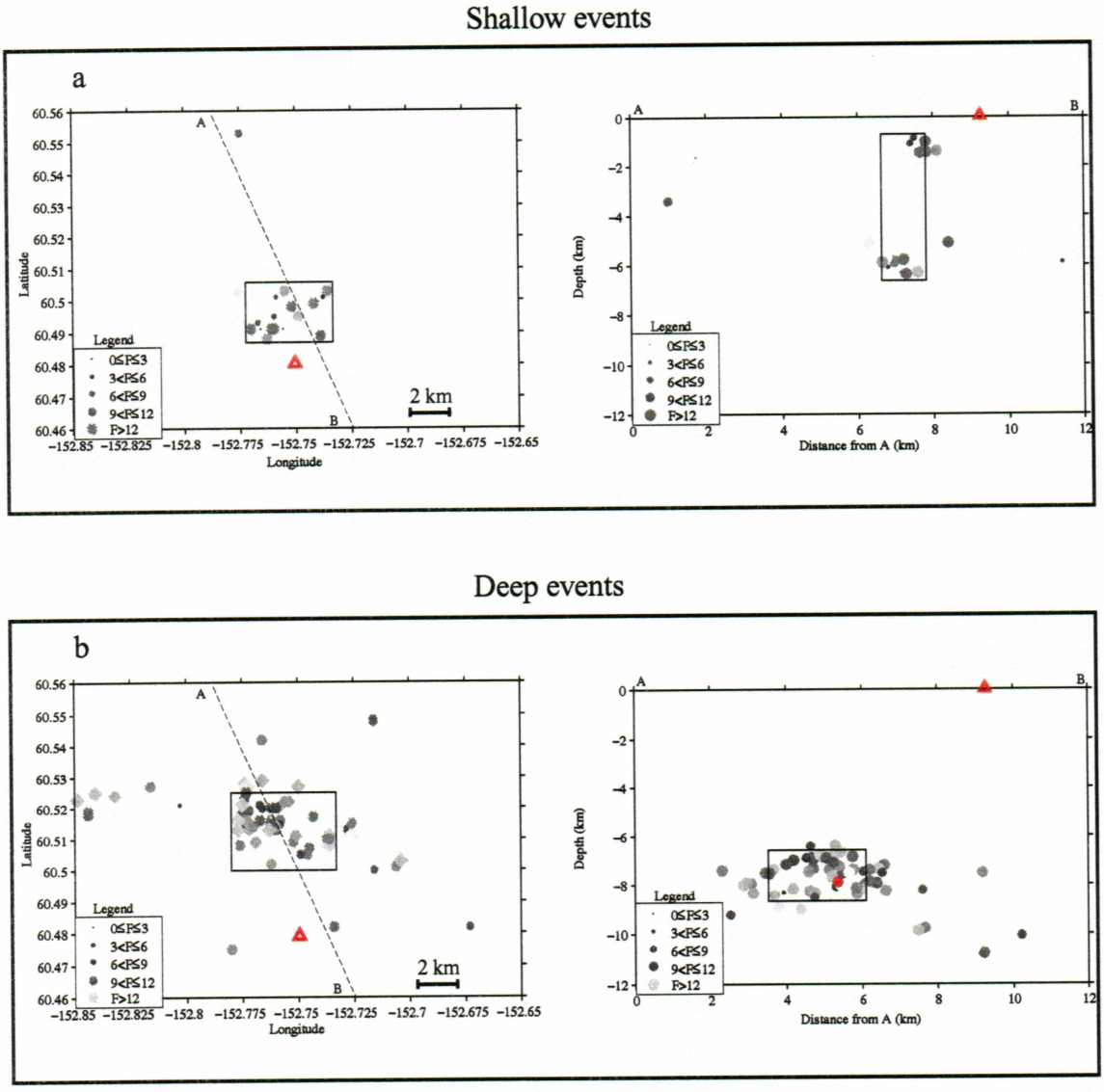

Figures 17. Maps of Individual Misfits for Each Phase Identified in Figure 15.
(a-b) Maps and cross-sections of misfits, during July 1991, for events within individual segments of figure 15. Boxes show the regions from which subsets of FPS were selected. Other conventions as in figures 9a-b.

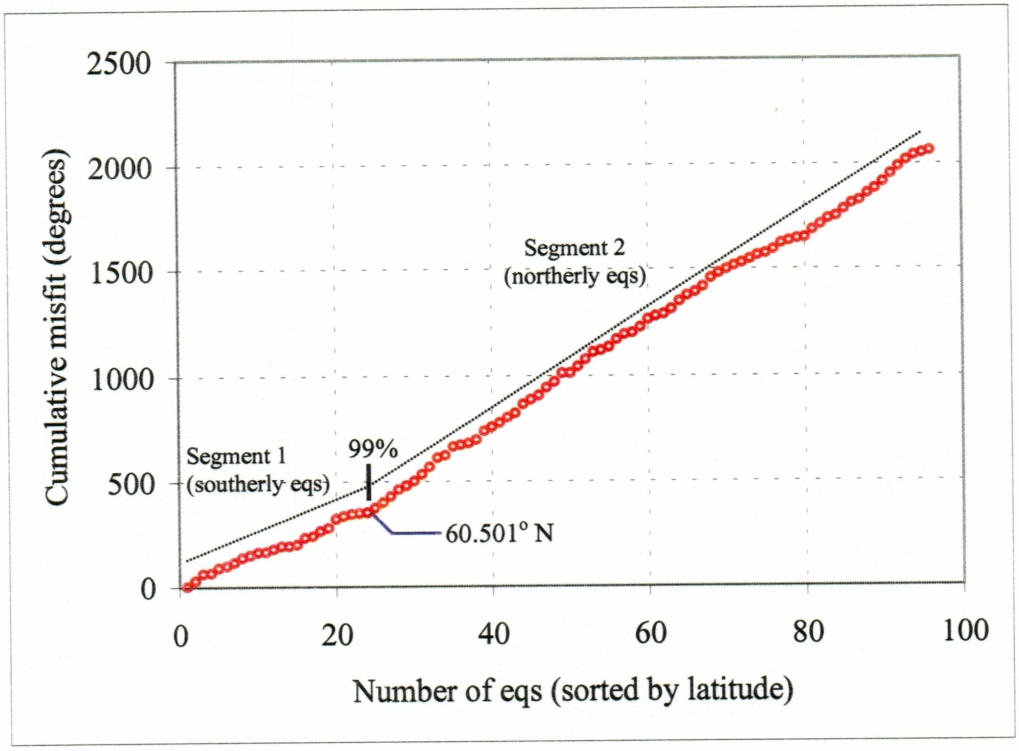

Figure 18. Cumulative Misfit vs. Latitude During July 1991. Cumulative misfit vs. number of earthquakes, ordered by latitude, for earthquakes during July 1991. Conventions as in figure 15.

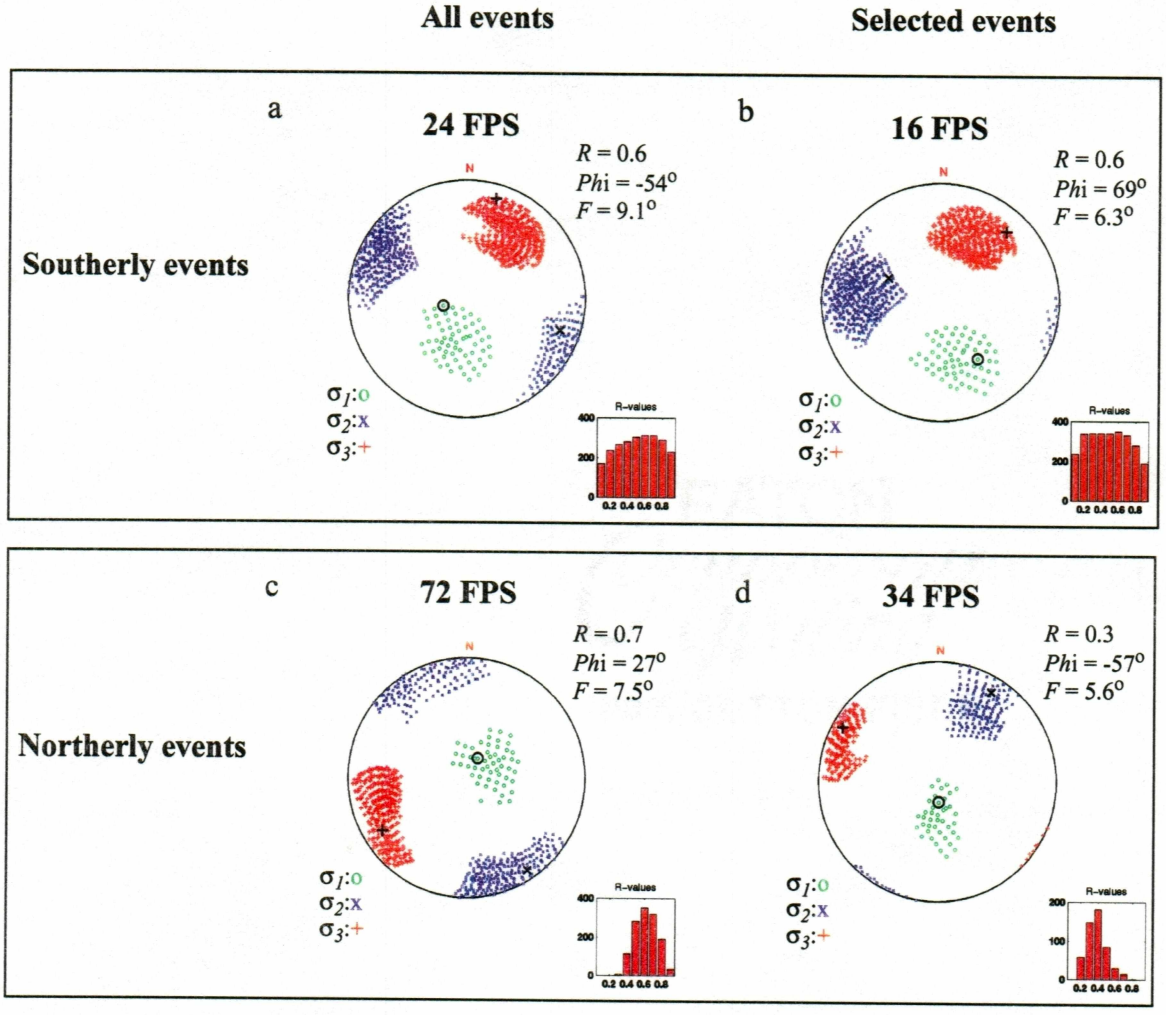

Figure 19. Principal Stress Directions as a Function of Latitude, July 1991.
(a-d) Stereographic projections of principal stress directions, during July 1991, estimated by inversions of FPS within individual segments of figure 18. Stress directions obtained by inverting all FPS (a, c) and subsets within each segment (b, d) are shown. Conventions as in figure 8.

Southerly events

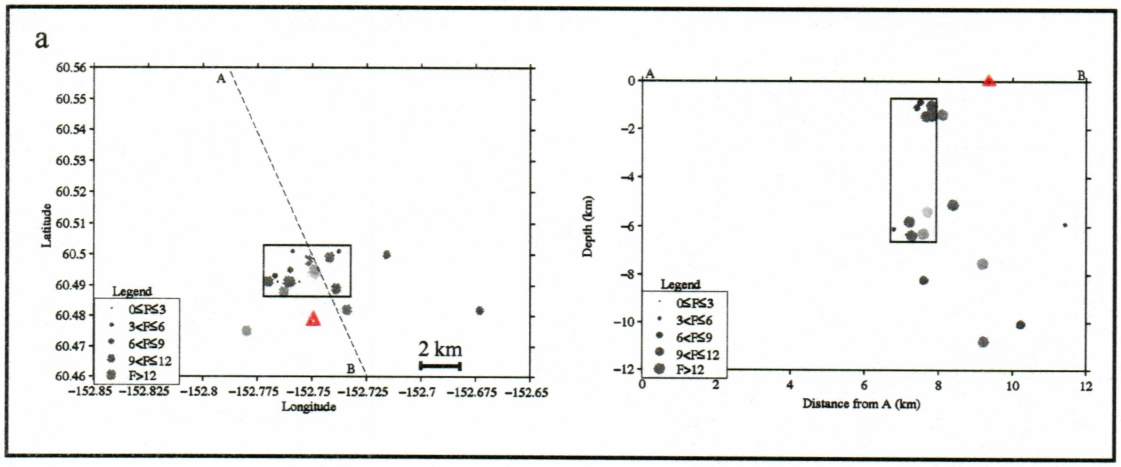

Northerly events

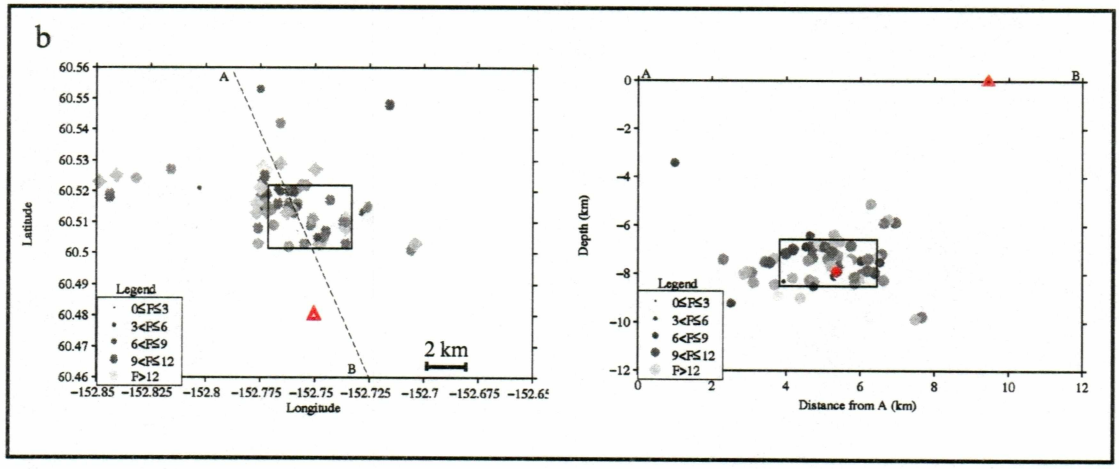

Figure 20. Maps of Individual Misfits for Each Phase Identified in Figure 18.
(a-b) Maps and cross-sections of misfits, during July 1991, for events within individual segments of figure 18. Boxes show the regions were subsets of FPS were selected from. Other conventions as in figures 9a-b.

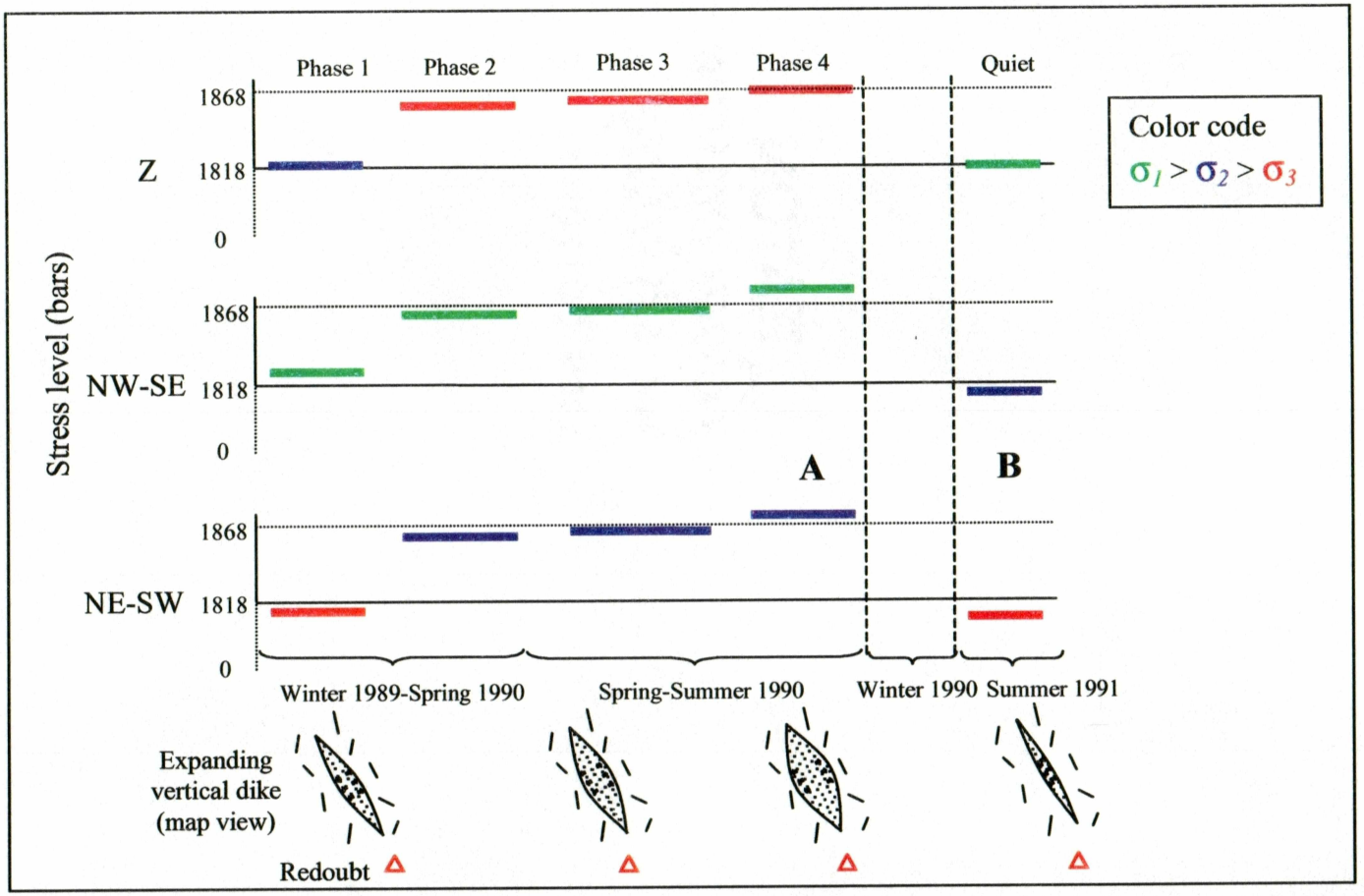

Figure 21. Change in Stress at Redoubt. Model I: Single Dike Expansion. Change in absolute and relative values of stress level near Redoubt. Plots of levels of stress in a fixed reference frame with axes oriented vertically, NW-SE and NE-SW. The assumed value of vertical load (overburden) is 1818 bars at 7 km depth (see discussion). Green, blue, and red lines are drawn at the approximate value of σ_1, σ_2, and σ_3 principal stresses during each phase of activity. Length of colored lines is proportional to duration of each phase. Vertical dotted lines show the period were no data was analyzed. Lower diagrams show a scheme of expansion and contraction of a dike, or tabular magma body (hatched region oriented NW-SW, map view). Solid lines around this oval represent randomly oriented faults. Red triangle marks the location of Redoubt volcano.

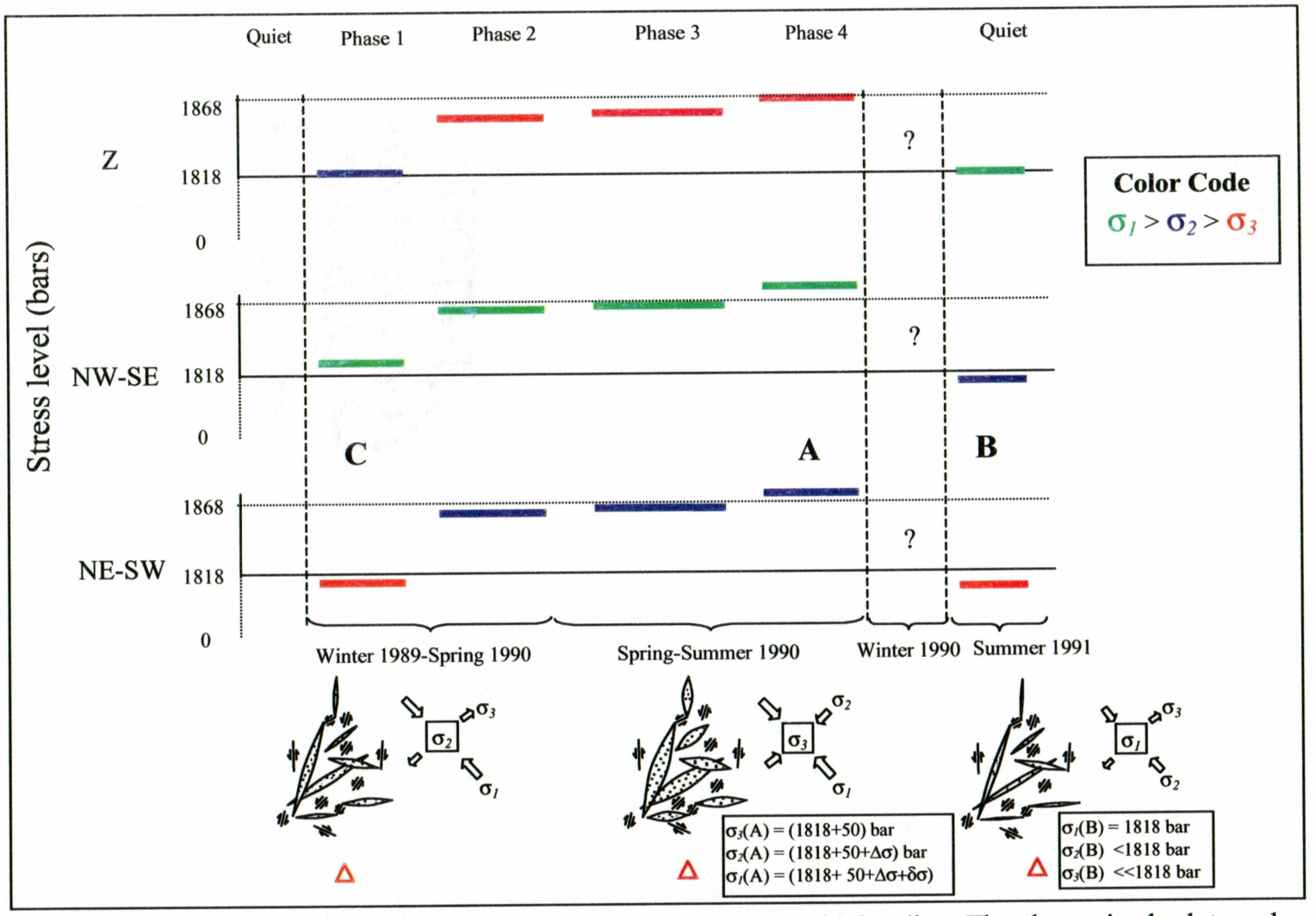

Figure 22. Change in Stress at Redoubt. Model II: Expansion of Multiple Dikes. The change in absolute and relative values of stress level near Redoubt is better explained by the expansion and contraction of a complex system of dikes and sills within the magma reservoir (sketch shown below). Conventions as in figure 21.

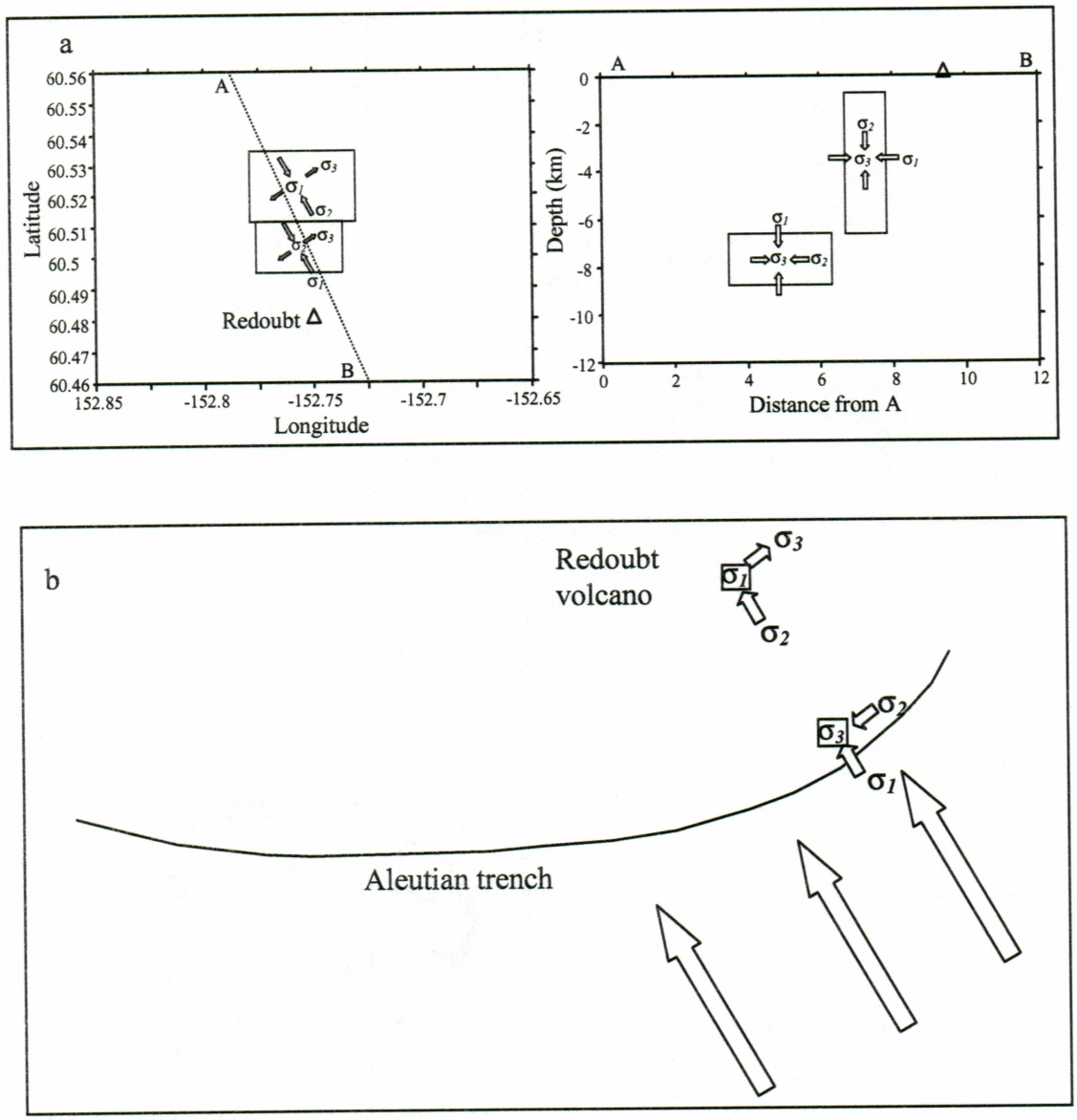

Figure 23. Local and Regional Orientation of Stresses. (a) Map and cross section of directions of stress estimated by inversion of FPS during July 1991. The general directions of stress as described in figures 17 and 20 are shown. Hollow arrows indicate principal stresses directions. Triangle marks the location of Redoubt volcano. Dotted line shows the orientation of cross section, shown to the right. Boxes enclose the regions sampled by earthquakes whose inversion yielded the lowest average misfits. (b) Sketch of the directions of principal stress near Redoubt, compared to expected stress directions resulting from plate collision. Large hollow arrows indicate direction of plate convergence.

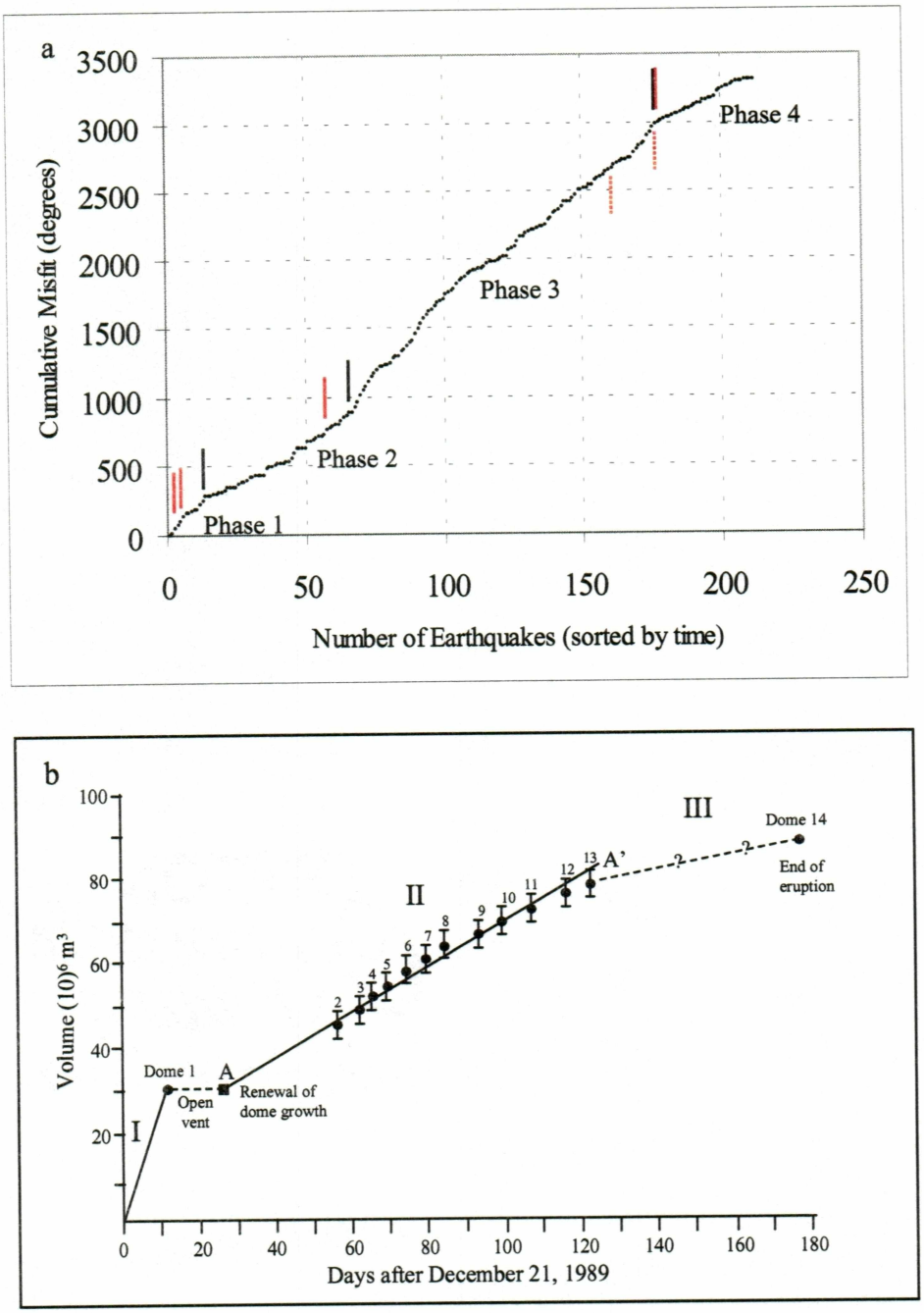

Figure 24. Change in Stress with Time and the Rate and Volume of Magma Supply. (a) Cumulative misfit vs. time (this thesis). Conventions as in figure 10. (b) Cumulative volume of andesitic dome material erupted at Redoubt volcano during dome-growth period extending from December 21, 1989, to mid June, 1990. I, II, and III refer to different segment of dome growth discussed in text. Error bars on volumes for domes 3-13 represent arbitrary estimates. A-A' is least-squares fit for domes 3-13. (Caption and figure From Miller, 1994).

References

Aki, K., and P. Richards, *Quantitative Seismology*, 573 pp., Freeman and Company, San Francisco, 1980.

Angelier, J., Determination of the mean principal directions of stresses for a given fault population, *Tectonophysics*, *56*, T17-T26, 1979.

Aspinall, W.P., A.D. Miller, L.L. Lynch, J.L. Latchman, R.C. Steward, R.A. White, and J.A. Power, Soufriere Hills eruption, Monserrat, 1995-1997: volcanic earthquake locations and fault plane solutions, *Geophys. Res. Lett.*, *25* (18), 3397-3400, 1998.

Barker, S.E., and S.D. Malone, Magmatic system geometry at Mount St. Helens modeled from the stress field associated with posteruptive earthquakes, *J. Geophys. Res.*, *96* (B7), 11883-11894, 1991.

Bautista, B.C., M.L. Bautista, R.S. Stein, E.S. Barcelona, R.S. Punongbayan, E.P. Laguerta, A.R. Rasdas, G. Ambubuyong, and E.Q. Amin, Relationship of regional and local structures to mount Pinatubo activity, in *Fire and Mud: Eruptions and lahars of mount Pinatubo, Philippines*, edited by C. Newhall, and R. Punongbayan, pp. 1120, University of Washington Press, Seattle, 1996.

Benz, H.M., B.A. Chouet, P.B. Dawson, J.C. Lahr, R.A. Page, and J.A. Hole, Three-dimensional P and S wave velocity structure of Redoubt Volcano, Alaska, *J. Geophys. Res.*, *101* (B4), 8111-8128, 1996.

Bianco, F., M. Castellano, G. Milano, G. Ventura, and G. Vilardo, The Somma-Vesuvius stress field induced by regional tectonics: evidences from seismological and mesostructural data, *J. Volcanol. Geotherm. Res.*, *82*, 199-218, 1998.

Bruno, G., I. Guerra, A. Moretti, and G. Neri, Space variations of stress along the Tyrrhenian Wadati-Benioff zone, *Pure and Applied Geophysics*, *156*, 667-688, 1999.

Caccamo, D., G. Neri, A. Sarao, and M. Wyss, Estimates of stress directions by inversion of earthquake fault-plane solutions in Sicily, *Geophys. J. Int.*, *125*, 857-868, 1996.

Casadevall, T.J., M.P. Doukas, C.A. Neal, R.G. McGimsey, and C.A. Gardner, Emission rates of sulfur dioxide and carbon dioxide from Redoubt Volcano, Alaska during the 1989-1990 eruptions, *J. Volcanol. Geotherm. Res.*, *62* (1-4), 519-530, 1994.

Chadwick, W.W.J., R.J. Archuleta, and D.A. Swanson, The mechanics of ground deformation precursory to dome-building extrusions at Mount St. Helens, 1981-1982, *J. Geophys. Res.*, *93*, 4351-4366, 1988.

Chouet, B.A., R.A. Page, C.D. Stephens, J.C. Lahr, and J.A. Power, Precursory swarms of long-period events at Redoubt Volcano (1989-1990), Alaska: Their origin and use as a forecasting tool, *J. Volcanol. Geotherm. Res.*, *62* (1-4), 95-135, 1994.

Cocina, O., G. Neri, E. Privitera, and S. Spampinato, Stress tensor computations in the Mount Etna area (southern Italy) and tectonic implications, *J. Geodynamics*, *23* (2), 109-127, 1997.

Cocina, O., G. Neri, E. Privitera, and S. Spampinato, Seismogenic stress field beneath Mt. Etna (South Italy) and possible relationships with volcano-tectonic features, *J. Volcanol. Geotherm. Res.*, *83*, 335-348, 1998.

Dawson, P.B., B.A. Chouet, J.C. Lahr, R.A. Page, J.R. VanSchaack, and E.E. Criley, Data report for a seismic study of the P and S wave velocity structure of Redoubt Volcano, Alaska, pp. 1-43, USGS, 1996.

Dawson, P.B., B.A. Chouet, R.A. Page, and J.C. Lahr, A post-eruptive seismic survey of Redoubt Volcano, Alaska, *Seism. Res. Lett.*, *63* (1), 67, 1992.

De Natale, G., S.M. Petrazzuoli, C. Troise, F. Pingue, and P. Capuano, Internal stress field at Mount Vesuvius: a model for background seismicity at a central volcano, *Journal of Gephysical Research*, *105* (B7), 16207-16214, 2000.

Etchecopar, A., G. Vasseur, and M. Daignieres, An inverse problem in microtectonics for the determination of stress tensor from fault striation analysis, *J. Struct. Geol.*, *3* (1), 51-65, 1981.

Falsaperla, S., G. Lanzafame, V. Longo, and S. Spampinato, Regional stress field in the area of Stromboli (Italy): insights into structural data and crustal tectonic earthquakes, *J. Volcanol. Geotherm. Res.*, *88*, 147-166, 1999.

Frepoli, A., G. Selvaggi, C. Chiarabba, and A. Amato, State of stress in the southern Tyrrhenian subduction zone from fault-plane solutions, *Geophys. J. Int.*, *125*, 879-891, 1996.

Gardner, C.A., C.A. Neal, R.B. Waitt, and R.J. Janda, Proximal pyroclastic deposits from the 1989-1990 eruption of Redoubt Volcano, Alaska - Stratigraphy, distribution, and physical characteristics., *J. Volcanol. Geotherm. Res.*, *62*, 213-250, 1994.

Gautneb, H., and A. Gudmundsonn, Effect of local and regional stress fields on sheet emplacement in West Iceland, *J. Volcanol. Geotherm. Res.*, *51*, 339-356, 1992.

Gephart, J.W., Principal stress directions and the ambiguity in fault plane identification from focal mechanisms, *Bull. Seismol. Soc. Am.*, *75* (2), 621-625, 1985.

Gephart, J.W., FMSI: a FORTRAN program for inverting fault/slickenside and earthquake focal mechanism data to obtain the regional stress tensor, *Comp. Geos.*, *16* (7), 953-989, 1990.

Gephart, J.W., Stress and the direction of slip on fault planes, *Tectonics*, *9* (4), 845-858, 1990.

Gephart, J.W., and D.W. Forsyth, An improved method for determining the regional stress tensor using earthquake focal mechanism data: application to the San Fernando earthquake sequence, *J. Geophys. Res.*, *89* (B11), 9305-9320, 1984.

Giampiccolo, E., C. Musumeci, S.D. Malone, S. Gresta, and E. Privitera, Seismicity and stress-tensor inversion in the central Washington Cascade Mountains, *Bull. Seismol. Soc. Am.*, *89* (3), 811-821, 1999.

Gillard, D., Principal stress orientations inferred from inversion of focal mechanism data in Hawaii and Iran, Ph.D. thesis, University of Alaska, Fairbanks, Fairbanks, 1993.

Gillard, D., Principal Stress Orientations Inferred From Inversion of Focal Mechanism Data in Hawaii and Iran, Ph.D. thesis, University of Alaska, Fairbanks, Fairbanks, 1993.

Gillard, D., and M. Wyss, A seismotectonic model for western Hawaii based on stress tensor inversion from fault plane solutions, *J. Geophys. Res.*, *97* (B5), 6629-6641, 1992.

Gillard, D., and M. Wyss, Comparison of strain and stress tensor orientation: application to Iran and southern California, *J. Geophys. Res.*, *100* (B11), 22197-22213, 1995.

Gillard, D., M. Wyss, and P. Okubo, Type of faulting and orientation of stress and strain as a function of space and time in Kilauea's south flank, Hawaii, *J. Geophys. Res.*, *101* (B7), 16025-16042, 1996.

Hanks, T.C., and C.B. Raleigh, The conference on magnitude of deviatoric stresses in the earth's crust and uppermost mantle, *Journal of Gephysical Research*, *85* (B11), 6083-6085, 1980.

Hardebeck, J.L., and E. Hauksson, Stress orientations obtained from earthquake focal mechanisms: what are appropriate uncertainty estimates?, *Bull. Seismol. Soc. Am.*, 2000.

Heleno da Silva, S.I., S.J. Day, and J.F. Fonseca, Fogo Volcano, Cape Verde Islands: seismicity-derived constraints on the mechanism of the 1995 eruption, *J. Volcanol. Geotherm. Res.*, *94*, 219-231, 1999.

Herrmann, R., A student's guide to the use of p and S wave data for focal mechanism determination, *Earthquake Notes*, *46* (4), 29-39, 1975.

Hill, D.P., A model for earthquake swarms, *J. Geophys. Res.*, *82* (8), 1347-1352, 1977.

Horiuchi, S., G. Rocco, and A. Hasegawa, Discrimination of fault planes from auxiliary planes based on simultaneous determination of stress tensor and a large number of fault plane solutions, *J. Geophys. Res.*, *100* (B5), 8327-8338, 1995.

Jolly, A.D., R.A. Page, and J.A. Power, Seismicity and stress in the vicinity of Mount Spurr volcano, south central Alaska, *J. Geophys. Res.*, *99* (B8), 15305-15318, 1994.

Kienle, J., S.E. Swanson, and H. Pulpan, Magmatism and subduction in the eastern Aleutian Arc, in *Arc volcanism : Physics and Tectonics*, edited by D. Shimozuru, and I. Yokohama, TERRAPUB, Tokyo, 1983.

Lahr, J.C., HYPOELLIPSE: A computer program for determining local earthquake hypocentral parameters, magnitude and first-motion pattern (Y2K compliant version), USGS, 1999.

Lahr, J.C., B.A. Chouet, C.D. Stephens, J.A. Power, and R.A. Page, Earthquake classification, location, and error analysis in a volcanic environment: implications for the magmatic system of the 1989-1990 eruptions at Redoubt volcano, Alaska, *J. Volcanol. Geotherm. Res.*, *62* (1-4), 137-151, 1994.

Lay, T., and T.C. Wallace, *Modern Global Seismology*, 521 pp., Academic Press, San Diego, 1995.

Lisle, R., New method of estimating regional stress orientations: applications to focal mechanism data of recent British earthquakes, *Geophys. J. Int.*, *110*, 276-282, 1992.

Locker, D.A., *Rock failure*. AGU reference shelf 3. Rock physics and phase relations. A handbook of physical constants. Thomas J. Ahrens (Ed). American Geophysical Union, 1995.

Lu, Z., and M. Wyss, Segmentation of the Aleutian plate boundary derived from stress direction estimates based on fault plane solutions, *J. Geophys. Res.*, *101* (B1), 803-816, 1996.

Lu, Z., M. Wyss, and H. Pulpan, Details of stress directions in the Alaska subduction zone from fault plane solutions, *J. Geophys. Res.*, *102* (B3), 5385-5402, 1997.

Martin, G.C., and F. Katz, J, A geologic reconnaissance of the Iliamna region, Alaska., U. S. Geological Survey, 1912.

McKenzie, D.P., The relation between fault plane solutions for earthquakes and the directions of the principal stresses, *Bull. Seismol. Soc. Am.*, *59* (2), 591-601, 1969.

McNutt, S.R., Some seismic precursors at Pavlof Volcano, Alaska, October 1973 - April 1986, in *IAVCEI Proceedings in Volcanology*, 1989.

McNutt, S.R., Seismic monitoring and eruption forecasting of volcanoes: A review of the state-of-the-art and case histories, in *Monitoring and mitigation of volcano hazards*, edited by G. Scarpa, and T. R, Springer Verlag, Berlin, 1996.

Michael, A.J., Determination of stress from slip data: faults and folds, *J. Geophys. Res.*, *89* (B13), 11517-11526, 1984.

Michael, A.J., Use of focal mechanisms to determine stress: a control study, *J. Geophys. Res.*, *92* (B1), 357-368, 1987.

Miller, T.P., Dome growth and destruction during the 1989-1990 eruption of Redoubt volcano, *J. Volcanol. Geotherm. Res.*, *62* (1-4), 197-212, 1994.

Minakami, T., Fundamental research for predicting volcanic eruptions (I)- Earthquakes and crustal deformations originating from volcanic activity, *Bulletin of the Earthquake Research Institute of the University of Tokyo*, *38*, 487-544, 1960.

Montone, P., A. Amato, C. Chiaraba, G. Buonasorte, and A. Fiordelisi, Evidencence of active extension in quaternary volcanoes of central Italy from breakout analysis and seismicity, *Geophys. Res. Lett.*, *22* (4), 1909-1912, 1995.

Moran, S.C., Seismicity at Mount St. Helens, 1987-1992: Evidence for repressurization of an active magmatic system, *J. Geophys. Res.*, *99* (B3), 4341-4354, 1994.

Moran, S.C., D.R. Zimbelman, and S.D. Malone, A model for the magmatic-hydrothermal system at Mount Rainier, Washington, from seismic and geochemical observations, *Bull. Volcanol.*, *61*, 425-436, 2000.

Muñoz, F., A. Nieto, and H. Meyer, Analysis of swarms of high-frequency seismic events at Nevado del Ruiz volcano, Colombia (January 1986 - August 1987): Development of a procedure, *J. Volcanol. Geotherm. Res.*, *41*, 327-354, 1990.

Nakamura, K., Volcanoes as possible indicators of tectonic stress orientation: principle and proposal, *J. Volcanol. Geotherm. Res.*, *2*, 1-16, 1977.

Nakamura, K., K.H. Jacob, and J.N. Davies, Volcanoes as possible indicators of tectonic stress orientation - Aleutians and Alaska, *PAGEOPH*, *115*, 87-112, 1977.

Nakamura, K., and S. Uyeda, Stress gradient in arc-back arc regions and plate subduction, *J. Geophys. Res.*, *85* (B11), 6419-6428, 1980.

Nuñez, F.J., and C. Sánchez, Stress field estimations for Colima volcano, Mexico, based on seismic data, *Bull. Volcanol.*, *60*, 568-580, 1999.

Pallister, J.R., D. Hoblitt, D. Crandel, and D. Mullineaux, Mount St. Helens a decade after the 1980 eruptions: magmatic models, chemical cycles, and a revised hazard assessment., *Bulletin of Volcanology*, *54*, 126-146, 1992.

Parker, R.L., and M.K. McNutt, Statistics for the one-norm misfit measure, *J. Geophys. Res.*, *85* (B8), 4429-4430, 1980.

Patane, G., A. Montalto, S. Imposa, and S. Menza, The role of regional tectonics, magma pressure, and gravitational spreading in earthquakes of the eastern sector of Mt. Etna Volcano (Italy), *J. Volcanol. Geotherm. Res.*, *61*, 253-266, 1994.

Power, J.A., J.C. Lahr, R.A. Page, B.A. Chouet, C.D. Stephens, D.H. Harlow, T.L. Murray, and J.N. Davis, Seismic evolution of the 1989-1990 eruption sequence of Redoubt Volcano, Alaska, *J. Volcanol. Geotherm. Res.*, *62* (1-4), 69-94, 1994.

Reasenberg, P.A., and D. Oppenheimer, FPFIT, FPPLOT, and FPPAGE: FORTRAN computer programs for calculating and displaying earthquake fault-plane solutions, USGS, 1985.

Refraction Technology, Inc. Refraction Technology Product Specification, REF TEK 72A- 02 Portable digital seismic data acquisition system, pp. 1-24, Refraction Technology, Inc., 1990.

Riehle, J.R., M.D. Fleming, B.F. Molnia, J.H. Dover, J.S. Kelley, M.L. Miller, W.J. Nokleberg, G. Plafker, and A.B. Till, Digital shaded-relief image of Alaska, U.S. Geological Survey, 1996.

Rivera, L., and A. Cisternas, Stress tensor and fault plane solutions for a population of earthquakes, *Bull. Seismol. Soc. Am.*, *80* (3), 600-614, 1990.

Robinson, M., XPICK user's manual v 3.1. Seismology lab of the Geophysical Institute University of Alaska, Fairbanks, Geophysical Institute University of Alaska, Fairbanks, Fairbanks, 1991.

Sapin, M., A. Hirn, J.C. Lepine, and A. Nercessian, Stress, failure and fluid flow deduced from earthquakes accompanying eruptions at Piton de la Fournaise volcano, *J. Volcanol. Geotherm. Res.*, *70*, 145-167, 1996.

Sbar, M.L., Delineation and interpretation of seismotectonic domains in Western North America, *J. Geophys. Res.*, *87* (B5), 3919-3928, 1982.

Scott, W.E., and R.G. McGimsey, Character, mass, distribution, and origin of tephra-fall deposits of the 1989-1990 eruption of Redoubt Volcano, south-central Alaska, *J. Volcanol. Geotherm. Res.*, *62*, 251-272, 1994.

Slejko, D., G. Neri, I. Orozova, G. Renner, and M. Wyss, Stress field in Friuli (NE Italy) from fault plane solutions of activity following the 1976 main shock, *Bull. Seismol. Soc. Am.*, *89* (4), 1037-1052, 1999.

Solomon, S.C., R.M. Richardson, and E.A. Bergman, Tectonic stress: models and magnitudes, *Journal of Gophysical Research*, *85* (B11), 6086-6092, 1980.

Stein, S., *Introduction to seismology, earthquakes and earth structure*, 554 pp., 1992.

Stephens, C.D., B.A. Chouet, R.A. Page, J.C. Lahr, and J.A. Power, Seismological aspects of the 1989-1990 eruptions at Redoubt Volcano, Alaska: the SSAM perspective, J. Volcanol. Geotherm. Res., 62 (1-4), 153-182, 1994.

Sturm, M., C. Benson, and P. Mackeith, Effects of the 1966-1968 eruptions of Mount Redoubt on the flow of the Drift Glacier, J. Glaciol., 32, 335-362, 1986.

Till, A.B., M.E. Yount, and M.L. Bevier, The geologic history of Redoubt Volcano, Alaska, J. Volcanol. Geotherm. Res., 62 (1-4), 11-30, 1994.

Ui, T., K. Nakamura, and K. Shibahashi, 1974 activity of Chokai volcano, Japan, *Bull. Volcanol.*, *40* (4), 1-8, 1976.

Warren, N.W., and G.V. Latham, An experimental study of thermally induced microfracturing and its relation to volcanic seismicity, *J. Geophys. Res.*, *75* (23), 4455-4464, 1970.

Watanabe, T., T. Koyaguchi, and T. Seno, Tectonic stress controls on ascent and emplacement of magmas, *J. Volcanol. Geotherm. Res.*, *91*, 65-78, 1999.

Waythomas, C.F., J.M. Dorava, T.P. Miller, C.A. Neal, and R.G. McGimsey, Preliminary volcano-hazard assessment for Redoubt volcano, Alaska, pp. 1-40, Alaska Volcano Observatory, Anchorage, 1998.

Wessel, P., and W. Smith, GMT, the Generic Mapping Tools. Technical Reference and Cookbook, Manoa, 1999.

Wiemer, S., and S.R. McNutt, Variations in the frequency-magnitude distribution with depth in two volcanic areas: Mount St. Helens, Washington, and Mt. Spurr, Alaska, *Geophys. Res. Lett.*, *24* (2), 189-192, 1997.

Wiemer, S., S.R. McNutt, and M. Wyss, Temporal and three-dimensional spatial analyses of the frequency-magnitude distribution near Long Valley Caldera, California, *Geophys. J. Int.*, *134*, 409-421, 1998.

Wiemer, S., and R. Zuñiga, ZMAP V 5.0. A software package to analyze seismicity, 1999.

Wyss, M., D. Gilliard, and B. Liang, An estimate of the absolute stress tensor in Kaoiki, Hawaii, *J. Geophys. Res.*, *97* (B4), 4763-4768, 1992.

Wyss, M., B. Liang, W.R. Tanigawa, and X. Wu, Comparison of stress and strain tensors based on fault plane solutions in Kaoiki, Hawaii, *J. Geophys. Res.*, *97* (B4), 4769-4790, 1992.

Wyss, M., and Z. Lu, Plate boundary segmentation by stress directions: Southern San Andreas fault, California, *Geophys. Res. Lett.*, *22* (5), 547-550, 1995.

Yin, Z.M., An improved method for the determination of the tectonic stress field from focal mechanism data, *Geophys. J. Int.*, *125*, 841-849, 1996.

Zoback, M.L., and M. Zoback, State of stress in the conterminous United States, *J. Geophys. Res.*, *85* (B11), 6113-6156, 1980.

Zobin, V., Focal Mechanism of volcanic earthquakes, *Bulletin Vulcanologique*, *36* (4), 517-522, 1972.

Zobin, V., The fault nature of the Ms 5.4 volcanic earthquake preceding the 1996 subglacial eruption of Grimsvotn Volcano, Iceland, *J. Volcanol. Geotherm. Res.*, *92*, 349-358, 1999.

Zollweg, J.E., Seismicity following the 1985 eruption of Nevado del Ruiz, Colombia, *J. Volcanol. Geotherm. Res.*, *41*, 355-367, 1990.

Appendix

Appendix A. Summary of Information About Data Used.

For 212 earthquakes recorded by AVO permanent network (Dec. 1989 - Dec. 1990)						
	STDR	Average Δstrike, Δdip, Δrake (degrees)	Number of Readings	Ndisc/Npol	ERH (km)	ERZ (km)
Range	0.41 - 0.84	0.00 - 32	6 - 14	0.00 - 0.20	0.40 - 3.20	1.10 - 3.70
Average	0.60	12.67	7	0.04	0.92	1.78
Comment	111 FPS with STDR above average	119 FPS with uncertainties below average	59 FPS with 8 or more readings	148 FPS with ratio below average	147 FPS with ERH below average	117 FPS with ERZ below average
For 96 earthquakes recorded during the deployment of July 1991						
Range	0.42 - 0.90	0.00 - 44.33	6 - 25	0.00 - 0.24	0.20 - 2.20	0.10 - 1.40
Average	0.72	16.42	10	0.04	0.38	0.63
Comment	60 FPS with STDR above average	53 FPS with uncertainties below average	33 FPS with 11 or more readings	63 FPS with ratio below average	55 FPS with ERH below average	66 FPS with ERZ below average

Appendix B. Focal Mechanims at Other Alaskan Volcanoes.

We used first motion data for earthquakes at four Alaskan volcanoes, namely, Pavlof, Dutton, Akutan and Makushin and computed composite focal mechanism solutions for groups of earthquakes recorded between August 1996 and September 1998. The composite focal mechanisms at the four volcanoes show considerable variation. For a group of three events at Pavlof volcano we found a composite solution that represents thrusting, with nodal planes striking WNW. This may represent dominantly compressional stresses prevailing in the area oriented about 40 degrees off the direction of plate convergence. At Dutton volcano, solutions were computed for two different clusters of earthquakes. The solution for a cluster located NW of the summit represents thrust faulting with the pressure axis oriented parallel to the direction of plate convergence. For Akutan volcano, the solution for a cluster located east of the volcano represents normal faulting with the pressure axis oriented orthogonal to the direction of plate convergence. The solution for another cluster located NW of the summit shows strike-slip faulting and pressure axis oriented in the E-W direction. Based on both of these observations we suggest that local stresses may dominate at Akutan volcano, since the P axes appear to be unrelated to plate convergence. At Makushin volcano we obtained constrained solutions for three clusters. For a cluster located NE of the summit we found strike-slip faulting with a normal component and the pressure axis nearly parallel to the direction of plate convergence. For the cluster located east of the summit, the solution is strike- slip faulting with the pressure axis oriented SE-NW (subparallel to plate

convergence). For a cluster located NW of Makushin's summit the composite solution shows thrust faulting with the pressure axis oriented SE-NW. Again this suggests local stresses superimposed on those due to plate convergence.